



Published in final edited form as:

*J Comput Neurosci*. 2011 October ; 31(2): 159–182. doi:10.1007/s10827-010-0303-y.

## Passive and active shaping of unitary responses from associational/commissural and perforant path synapses in hippocampal CA3 pyramidal cells

**Tamara Perez-Rosello,**

Department of Neuroscience, University of Pittsburgh, Pittsburgh, PA, USA

**John L. Baker,**

Center for Neural Informatics, Structure, & Plasticity, and Molecular Neuroscience Department, Krasnow Institute for Advanced Study, George Mason University, 4400 University Drive, MS 2A1, Fairfax, VA 22030, USA

**Michele Ferrante,**

Center for Neural Informatics, Structure, & Plasticity, and Molecular Neuroscience Department, Krasnow Institute for Advanced Study, George Mason University, 4400 University Drive, MS 2A1, Fairfax, VA 22030, USA

**Satish Iyengar,**

Department of Statistics, University of Pittsburgh, Pittsburgh, PA, USA

**Giorgio A. Ascoli, and**

Center for Neural Informatics, Structure, & Plasticity, and Molecular Neuroscience Department, Krasnow Institute for Advanced Study, George Mason University, 4400 University Drive, MS 2A1, Fairfax, VA 22030, USA

**Germán Barrionuevo**

Department of Neuroscience, University of Pittsburgh, Pittsburgh, PA, USA

Giorgio A. Ascoli: [ascoli@gmu.edu](mailto:ascoli@gmu.edu)

### Abstract

Although associational/commissural (A/C) and perforant path (PP) inputs to CA3b pyramidal cells play a central role in hippocampal mnemonic functions, the active and passive processes that shape A/C and PP AMPA and NMDA receptor-mediated unitary EPSP/EPSC (AMPA and NMDA uEPSP/uEPSC) have not been fully characterized yet. Here we find no differences in somatic amplitude between A/C and PP for either AMPA or NMDA uEPSPs. However, larger AMPA uEPSCs were evoked from proximal than from distal A/C or PP. Given the space-clamp constraints in CA3 pyramidal cells, these voltage clamp data suggest that the location-independence of A/C and PP AMPA uEPSP amplitudes is achieved in part through the activation of voltage dependent conductances at or near the soma. Moreover, similarity in uEPSC amplitudes

---

© Springer Science+Business Media, LLC 2010

Correspondence to: Giorgio A. Ascoli, [ascoli@gmu.edu](mailto:ascoli@gmu.edu).

*Present Address:* T. Perez-Rosello Department of Otolaryngology, University of Pittsburgh School of Medicine, Pittsburgh, PA, USA

#### Author contributions

All of the authors have contributed to this study. GAA and GB conceived the conceptual framework of the study. TPR, JLB, MF, GAA, and GB conceived and designed the experiments. Experiments were performed by TPR at University of Pittsburgh. JLB, MF, TPR, IS, GAA, GB analyzed and interpreted the data. TPR, JLB, MF, IS, GAA, and GB drafted the article.

Electronic supplementary material The online version of this article (doi:10.1007/s10827-010-0303-y) contains supplementary material, which is available to authorized users.

for distal A/C and PP points to the additional participation of unclamped active conductances. Indeed, the pharmacological blockade of voltage-dependent conductances eliminates the location-independence of these inputs. In contrast, the location-independence of A/C and PP NMDA uEPSP/uEPSC amplitudes is maintained across all conditions indicating that propagation is not affected by active membrane processes. The location-independence for A/C uEPSP amplitudes may be relevant in the recruitment of CA3 pyramidal cells by other CA3 pyramidal cells. These data also suggest that PP excitation represents a significant input to CA3 pyramidal cells. Implication of the passive data on local synaptic properties is further investigated in the companion paper with a detailed computational model.

## Keywords

AMPA receptor; NMDA receptor; Hippocampus

## 1 Introduction

Hippocampal area CA3 is critically involved in the rapid encoding of new contextual memories, spatial working memory, and in pattern separation (cf. Kesner 2007; Leutgeb et al. 2007; Rolls 2007). The implementation of rapid encoding by area CA3 may be related to several distinctive connectivity features. Specifically, CA3 pyramidal cells receive two external excitatory inputs from the entorhinal cortex (EC). The most important input is conveyed monosynaptically via the PP, the axons of stellate cells in EC layer II. PP fibers make synaptic contacts on the distal apical dendrites in str. lacunosum-moleculare (Steward 1976; Witter and Amaral 1991). The second input from EC is conveyed disynaptically via the mossy fibers (MF), the axons of the dentate gyrus granule cells, which in turn receive input from the same layer II cells in EC (Steward 1976; Witter and Amaral 1991). The MF synapse is located on the apical dendrite in str. lucidum proximal to the cell soma (Blackstad et al. 1970; Claiborne et al. 1986). Another distinctive connectivity feature of area CA3 is that pyramidal cells receive strong recurrent (feedback and feed-forward) excitation via the extensive network of associational/commissural (A/C) input from other CA3 pyramidal cells (Ishizuka et al. 1990; Li et al. 1994). A/C axons target both the apical dendrites in str. radiatum and basal dendrites in str. oriens (Ishizuka et al. 1990; Li et al. 1994).

Pyramidal cells fire action potentials when the membrane potential reaches threshold through integration of excitatory synaptic responses generated at different distances from the soma. The dendritic propagation of synaptic responses is controlled, in part, by the passive cable properties of the cell's membrane (Jack et al. 1971; Rall 1967), which attenuate the amplitude and prolong the time course of the synaptic waveforms. In principle, synaptic responses generated closer to the soma would have a larger impact on the pyramidal cell firing. However, the active properties of the dendritic membrane also can affect synaptic integration via activation of a wide variety of ligand- and voltage-dependent conductances (VDC) (Magee and Johnston 1995; Stuart and Sakmann 1995; cf. Johnston and Narayanan 2008; Williams and Stuart 2003). Synaptic scaling is other mechanism that could compensate for the voltage attenuation imposed by dendritic cable properties, making the unitary response amplitude independent of its dendritic origin (Andrasfalvy and Magee 2001; Nicholson et al. 2006; Smith et al. 2003, cf. Johnston and Narayanan 2008). Another mechanism that could affect the propagation is the passive normalization (Chitwood et al. 1999; Jaffe and Carnevale 1999; Nevian et al. 2007) in which the anatomic and "passive" biophysical properties of the cell coalesce to remove most of the dependence of somatic EPSP amplitude on synaptic location.

Despite the central role of CA3 pyramidal cells in learning and memory, most of the findings about synaptic propagation have been obtained in CA1 pyramidal neurons mainly because dendrite patch clamp recordings from those neurons are feasible (Johnston and Narayanan 2008). Unfortunately distal dendrites of CA3 pyramidal cells are difficult to visualize in the slice, thus making technically unfeasible the recordings of dendritic EPSP in these cells. An indirect method to study the dendrite propagation of synaptic responses is the combination of experimentally somatic recordings with computational models that use a realistic geometry of CA3 pyramidal cells. Previous studies using this approach showed slower kinetics for A/C than for MF responses and predicted strong passive attenuation of PP responses (Spruston et al. 1993; Williams and Johnston 1991). Although the involvement of some active conductances in shaping of the synaptic responses in CA3 pyramidal cells is known (Miles and Wong 1986; Urban and Barrionuevo 1998; Urban et al. 1998; Williams and Johnston 1991) there have been not studies exploring the effects of active mechanisms shaping A/C and PP EPSP/EPSC in the same cell. The passive models of CA3 pyramidal cells current available (Johnston and Brown 1983; Henze et al. 1996; Major et al. 1994; Spruston et al. 1993) do not use realistic synaptic responses for constraining the parameters of the model. In part, this is due to lack of experimental recordings from A/C and PP synaptic responses under passive conditions (pharmacological blockade of voltage-dependent conductances).

A further issue complicating the analysis of dendritic propagation is that glutamatergic responses are mediated by both AMPA and NMDA receptors (Berzhanskaya et al. 1998; Debanne et al. 1998; Jonas et al. 1993; McBain and Dingledine 1992; Spruston et al. 1995; Weisskopf and Nicoll 1995), which have different amplitudes and kinetics. Given its faster kinetics, it is likely that the AMPA component would be strongly attenuated by dendritic filtering as it propagates to the soma (Johnston and Brown 1983; Major et al. 1994; Spruston et al. 1993). Currently, there are no available data on the involvement of dendritic filtering on the shaping of A/C and PP AMPA and NMDA responses.

The implementation of a realistic model of synaptic integration and firing by CA3 pyramidal cells requires quantitative information of the unitary responses. Whereas the unitary properties of the MF synapse have been previously characterized (Jonas et al. 1993; Lawrence et al. 2004), the availability of a detailed analysis of A/C and PP AMPA and NMDA receptor-mediated unitary EPSP/EPSC (AMPA and NMDA uEPSP/uEPSC) is limited (Debanne et al. 1998; Miles and Wong 1986).

In the present experimental study and in the companion modeling paper we used a combined experimental and modeling approach to study the propagation of the AMPA and NMDA uEPSP/uEPSC from PP and A/C inputs. We provide a characterization of the amplitude and kinetic parameters of minimally evoked isolated AMPA and NMDA components from each of these two pathways recorded at the soma of pyramidal cells from the middle of area CA3 (CA3b). To test the hypothesis that synaptic propagation of PP and A/C in CA3 pyramidal cells is affected by active membrane properties (Miles and Wong 1986; Williams and Johnston 1991; Urban and Barrionuevo 1998; Urban et al. 1998), we studied the amplitude and kinetics of the isolated AMPA and NMDA components in current clamp (CC) and voltage clamp recording conditions. Understanding the passive and active properties that might affect PP and A/C inputs propagation would provide important insights about the role of these pathways in hippocampal function. To further dissect the contribution of active conductances unaffected by voltage clamp, synaptic responses at the soma were also measured under pharmacological blockage of voltage-dependent channels. The experimental somatic responses recorded under passive conditions were used to construct a realistic model of passive propagation of responses in the CA3b pyramidal cell, which is described in the companion paper (Baker et al. 2010). Using this model other mechanisms that may

affect the propagation of AMPA and NMDA uEPSP/uEPSC (e.g. synaptic scaling and passive normalization) are further examined.

## 2 Methods

### 2.1 Slices preparation

Animal use was in accordance with the University of Pittsburgh Institutional Animal Care and Use Committee. Male Sprague Dawley rats ( $23 \pm 5$  days old; Zivic–Miller Laboratory) were anaesthetized (Nembutal, I.P., 5 mg per 100 g body weight) and perfused intracardially with a modified artificial cerebrospinal fluid (ACSF) (concentrations in mM): 229 sucrose, 1.9 KCl, 1.2  $\text{Na}_2\text{HPO}_4$ , 26  $\text{NaHCO}_3$ , 10.0 glucose, 1.0  $\text{CaCl}_2$ , 4  $\text{MgCl}_2$ , 0.4 of ascorbic acid at  $4^\circ\text{C}$ ; pH 7.4 maintained with bubbled  $\text{O}_2$  (95%)/ $\text{CO}_2$  (5%) at room temperature. After perfusion, animals were decapitated, and the brains removed. Brain slices 315–400  $\mu\text{m}$  were cut using a vibrating Leica VT1000S and transferred to an incubation chamber with ACSF containing the following (in mM): 125 NaCl, 1.87 KCl, 12.5  $\text{Na}_2\text{HPO}_4$ , 26  $\text{NaHCO}_3$ , 2.17  $\text{CaCl}_2$ , 1.44  $\text{MgSO}_4$ , 10 glucose, saturated with 95%  $\text{O}_2$ /5%  $\text{CO}_2$ , pH 7.4. Slices were first preincubated at  $34^\circ\text{C}$  for 35 min and then maintained for at least 30 min at room temperature. The slices were individually transferred to a submersion recording chamber and superfused at constant flow ( $2.5 \text{ ml min}^{-1}$ ) with the following solution (in mM): 125 NaCl, 3.0 KCl, 1.25  $\text{Na}_2\text{HPO}_4$ , 25  $\text{NaHCO}_3$ , 2.0  $\text{CaCl}_2$ , 1.0  $\text{MgCl}_2$ , 10 glucose, pH 7.4. Bath perfusion temperature was maintained at  $32 \pm 1^\circ\text{C}$ .

### 2.2 Whole cell recordings

Whole-cell CC and VC recordings from CA3b pyramidal cells were obtained with the aid of infrared differential interference contrast (DIC) video microscopy. The  $\text{GABA}_A$ / $\text{GABA}_B$  receptors were routinely blocked using bath applied (–)–bicuculline methobromide, 10  $\mu\text{M}$  and CGP35348, 500  $\mu\text{M}$  or 2-hydroxysaclofen, 200  $\mu\text{M}$ . The AMPA- and NMDA uEPSP/uEPSC were isolated with bath applied D (–)–2-amino-5-phosphonopentanoic acid (D-APV; 50  $\mu\text{M}$ ) or 6-cyano-7-nitroquinoxaline-2, 3-dione (CNQX; 20  $\mu\text{M}$ ), respectively. In the majority of the experiments in which the NMDA component was isolated, the  $\text{Mg}^{2+}$  concentration in the external solution was decreased to 50  $\mu\text{M}$ . The patch electrodes (3–6  $\text{M}\Omega$ ) were filled with (in mM): 120 K-methylsulphate, 10 KCl, 10 Hepes, 0.2 EGTA, 4 ATP-Mg, 0.3 GTPNa, 14 phosphocreatine, 0.25% biocytin. In most cases, synaptic responses were obtained in three different recording conditions: 1) CC; 2) VC; and 3) passive VC. In passive VC experiments, the pipette solution contained Cs-methanesulfonate (120 mM) instead of K-methylsulphate, and QX-314 (5 mM) to block  $\text{K}^+$  and  $\text{Na}^+$  currents. QX-314 may block also the hyperpolarization-activated ( $I_h$ ) and  $\text{Ca}^{2+}$  conductances (Perkins and Wong 1995; Talbot and Sayer 1996). In passive VC experiments  $\text{Ni}^{2+}$  was also added to the bath to block  $\text{Ca}^{2+}$  currents. Recordings were performed with an Axopatch 200B amplifier (Molecular Devices, Sunnyvale, CA, USA), low pass filtered at 2 kHz and digitized at 10 kHz with a Digidata 1422 (Molecular Devices) interface. Step protocols and data acquisition were made with the Clampex software (Molecular Devices). CA3 pyramidal cells had stable resting potential within  $-75$  and  $-60$  mV (cells with more positive resting potential were discarded). Cells with high spontaneous activity were rejected because of “contamination” of the evoked responses. A series of inward and outward current steps (500 ms duration; 20 pA increments) were injected via the whole-cell pipette to assess input resistance ( $R_N$ ) (Fig. 1c).  $R_N$  was calculated as the slope of linear fit between voltage and injected current. The membrane time constant ( $\tau_m$ ) was calculated from the exponential fit of activation of hyperpolarizing responses. The amplitude of action potential was determined as the difference between peak and threshold voltages. The spike adaptation ratio (AR) of the first to last interspike interval within a sweep was quantified upon a depolarizing step of 100–500 pA. Based on this measure, CA3 pyramidal cells were

classified as strongly adapting ( $AR < 0.5$ ) or weakly adapting ( $0.5 < AR < 0.8$ ). Cells were discarded if changes in series resistance were more than 20%. Only recordings with noise levels (peak-to-peak) of less than 100  $\mu\text{V}$  (CC) or 5.0 pA (VC) were accepted. The mean peak-to-peak baseline noise level was of  $60 \pm 10 \mu\text{V}$  (range: 30–90  $\mu\text{V}$ ) and  $1.6 \pm 0.8 \text{ pA}$  (range: 0.1–4.2 pA) in CC and VC recording modes, respectively. The low baseline noise made possible to detect unitary responses as small as 0.03 mV or 1.8 pA.

### 2.3 Minimal stimulation techniques

EPSPs and EPSCs were evoked by minimal stimulation (Dobrunz et al. 1997; Raastad 1995) using extracellular stimulating electrodes (concentric bipolar CBAPB125; FHC, Inc., ME, USA). Brief (50–100  $\mu\text{s}$ ) stimulation pulses with intensities of 10 to 30  $\mu\text{A}$  and 80 to 120  $\mu\text{A}$  for A/C and PP respectively, were delivered at 0.2 Hz. The stimulation intensity was increased until minimal EPSPs/EPSCs were evoked at reliable failure rates of 40 to 60%. At these failure rates, the average amplitude of EPSPs/EPSCs (excluding failures) did not change by small changes in the stimulation intensity. Experiments with lower failure rate were rejected. Further criteria for recording of minimal responses were limited latency (<10 ms), and monoexponential EPSP decay. AMPA and NMDA uEPSP/uEPSC were evoked using similar strength of stimulation intensities. Supplementary Figure 1 illustrates the peak value (PV), dependency of individual A/C and PP AMPA and NMDA uEPSP from the stimulation intensity in four different cells showing a clear gap between failures and minimal responses. The stimulation sites were localized in CA3 str. radiatum, and in str. lacunosum moleculare on the border of the subiculum and area CA1, to activate A/C and PP fibers, respectively (Fig. 1a, b). In the str. radiatum, A/C responses were evoked from stimulations in proximal, medial, and distal locations (150–200  $\mu\text{m}$ , 200–250  $\mu\text{m}$ , and 250–300  $\mu\text{m}$  from str. pyramidale, respectively; Fig. 1a, b).

### 2.4 Drugs

(–)-bicuculline methobromide ( $\text{GABA}_A$  receptor antagonist, 10  $\mu\text{M}$ ); D(–)-2-amino-5-phosphonopentanoic acid (D-AP5, NMDA receptor antagonist, 50  $\mu\text{M}$ ), 6-cyano-7-nitroquinoxaline-2,3-dione (CNQX, an AMPA/kainate receptor antagonist, 10  $\mu\text{M}$ ); CGP35348 (500  $\mu\text{M}$ ) and 2-hydroxysaclofen (200  $\mu\text{M}$ ) ( $\text{GABA}_B$  receptor antagonists); QX314 (blocker of  $\text{Na}^+$ ,  $\text{K}^+$ ,  $\text{Ca}^{2+}$ , and  $\text{I}_h$  currents), were all purchased from Tocris, UK.  $\text{NiCl}_2$  (blocker of  $\text{Ca}^{2+}$  current) was from Sigma-Aldrich.

### 2.5 Analysis of stimulation-evoked EPSC and EPSP

EPSPs/EPSCs were recorded at 10 KHz. Consecutive data sweeps with representative data identified by the experimenter were converted into comma-separated-variables file format and loaded into R (R Development Core Team 2008) for processing. The response parameters (Fig. 2) were extracted using a combination of automatic and manual procedures. Here we provide a comprehensive description of this analysis, but the more pedantic details of this procedure and the related numerical parameters are reported at the end of the paper in the Appendix and Table 1, respectively. To ensure full reproducibility and further applications and extensions, we are also distributing the R source code freely upon request.

Processing of each data sweep was performed as follows. 1) The stimulus artifact was identified by searching a time interval around the expected time of stimulation and determining the largest magnitude second derivative of the signal; 2) The stimulus artifact was removed within a small time window around the time of stimulation and replaced with a linear interpolation spanning the period immediately before and after the stimulation; 3) The resting potential was estimated using a trimmed mean of values over an interval preceding the stimulation; 4) Noise reduction was applied by smoothing the response with a finite-impulse-response digital filter of minimal window size (one cycle before and after the

smoothing point) and a smoothing cutoff frequency (Table 1) determined by the type of data analyzed; 5) Latency, rise-time, time-to-peak (TTP), peak time, peak value, half-height width (HHW), and decay time constant parameters were estimated from the smoothed response; 6) The sweep was categorized as either rejected, failure, single-peak response, multi-peak response or an undetermined response type; 7) Finally, unitary responses were identified from among the single-peak responses based on the failure rate in the binomial approximation. These steps, explained in more detail below, are illustrated in Fig. 2 and Supplementary Figures 2 and 3.

Latency was first estimated directly from sweep data by linearly extrapolating the signal change from 20% to 80% of the peak back to the initial deviation from rest (Fig. 2). Latency was also derived as a parameter of the dual-exponential fitting procedure used to identify single-peak responses (see Appendix). Rise-time was defined as the time from 20% to 80% of peak (Fig. 2). Peak time is the time from stimulus artifact to actual response peak, whereas time-to-peak is defined here as the peak time minus the positive part of any estimated latency (Fig. 2). Half-height width is the time from the latest crossing of the half-peak amplitude prior to the peak to the earliest half-peak crossing following the peak (Fig. 2). Because of the sampling interval granularity (0.1 ms), crossing times were estimated by linear interpolation. The decay time constant was estimated using response values from the last 80% of the time interval from the peak to the falling half-height crossing (see Appendix for further details).

Sweeps were categorized as rejected, failure, single-peak response, multi-peak response, or undetermined based on several parameters, whose definition and numerical values are specified in the Appendix and in Table 1, respectively (see also Supplementary Figure 3). Other cases were generally categorized as undetermined, although the reader is referred to the Appendix for a comprehensive description of this procedure. Among the 16 experimental combinations of CC vs. VC, A/C vs. PP, and synaptic receptor blockers, the mean percentages of sweeps by category prior to the application of any manual category overrides were  $12\pm 1\%$ ,  $8\pm 1\%$ ,  $31\pm 3\%$ ,  $19\pm 1\%$ , and  $30\pm 3\%$  for rejected, undetermined, failure, multi-peak, and single-peak categories, respectively.

For sweeps categorized as single-peak responses, the response may arise from unitary synaptic activations or from multiple concurrent synaptic activations. After all sweeps in a consecutive group had been categorized, putative unitary sweeps in this group were identified based on a probability model of responses. Assumptions of the model are: 1) multiple synapses are potentially stimulated; 2) each synapse has an unchanging and equal probability of stimulation; 3) activated synapses have similar peak responses; and 4) peak values from multiple activations are approximately additive. For a fixed number of potentially stimulated synapses, the number activated would form a binomial distribution. Because the number of potential synapses is unknown, a Poisson limit was used to estimate the number of single activations given an observed failure rate. The failure rate was estimated as the number of categorized failures divided by the sum of the failures, single-peak responses, and multi-peak responses. Rejected sweeps and those of undetermined category were not used in estimating the number of single activations. For an estimated failure rate  $p$ , the number of expected unitary activations  $u$  is given by the formula:

$$u = -\log(p) \frac{p}{1-p} n$$

where  $n$  is the number of identified single-peak responses. Using the estimated number of unitary activations, putative unitary sweeps were identified by ranking peak amplitudes from

single-peak responses and taking the unitary sweeps from sweeps with the lowest peak value magnitudes (Supplementary Figure 2b). Response parameters of putative unitary sweeps are then summarized in terms of sample mean and s.d. and individually identified for further statistical analysis. This method to select unitary inputs was validated with a post-hoc analysis of simulated passive conditions using a computational model constrained by the experimental results, described in the companion paper (Baker et al. 2010). In terms of the overall fraction of unitary sweeps by experiment type, the lowest fraction of unitary sweeps after application of any manual overrides was in CC A/C NMDA experiments (7%) and the highest fraction was in CC A/C AMPA experiments (17%). Across all experimental types, the mean percentage of unitary sweeps was  $13\% \pm 1\%$ .

## 2.6 Additional statistical analysis

The statistical analyses on the unitary responses after sweep categorization and selection were carried out using the MINITAB (Minitab Inc, State College, PA, USA) and SAS packages (SAS Institute Inc, Cary, NC, USA). The main summaries are given as mean $\pm$ s.d., coefficient of variation, CV (CV=s.d./mean), and correlation (r). For comparison of various outcomes (e.g., PV, TTP, HHW) between pathways (e.g., A/C vs. PP) and between recording conditions (VC vs. passive VC) we used a random effects model to account for potential heterogeneity among the cells:

$$Y = m + E_p + E_c + I + e$$

Specifically, we regard the pathway as a fixed effect ( $E_p$ ) and the cell itself as a random effect ( $E_c$ ); we included a term to model (also as a random effect) the potential interaction ( $I$ ) between these main effects.  $Y$  is the outcome,  $m$  is the grand mean of the outcome across the data set, and  $e$  is the unexplained variation. For comparison of paths within a particular cell, we used a simpler fixed effects model.

## 3 Results

To study the active and passive dendritic propagation of AMPA and NMDA uEPSP/uEPSC in CA3 pyramidal cells, we compared the amplitudes and kinetics of EPSP/EPSCs evoked from stimulation sites in the str. radiatum of CA3 (for A/C responses), and from the str. lacunosum-moleculare (for PP responses) (Fig. 1a, b). Although most of the kinetic analyses are based on TTP and HHW, we also measured the rise-time and decay time constant (see Tables 2, 3 and 4). The majority of unitary synaptic responses were obtained in CC and VC recording conditions. In several experiments, we also compared unitary responses recorded in VC vs. passive VC conditions (see Section 2) to determine whether conductances located near the soma shape A/C and PP synaptic responses. The comparison of amplitude and kinetic parameters of uEPSC in VC vs. passive VC condition also gives information about conductances located distally from the soma that could be affecting the propagation of subthreshold responses. Furthermore, recordings under passive VC condition would also allow the construction of an adequately constrained passive computational model, which is described in the companion paper (Baker et al. 2010).

AMPA and NMDA uEPSP/uEPSC from A/C and PP synapses were obtained from 76 CA3 pyramidal cells. Most of the cells exhibited a strongly adapting train of action potentials in response to a depolarizing current injection (adaptation ratio:  $0.46 \pm 0.22$  (N=60); Fig. 1c; top trace). Overall, weakly-adapting cells comprised 30% of the data set whereas 55% of cells were strongly adapting. The remaining 15% of cells presented burst firing (Hemond et al. 2008). The properties of action potential waveforms were similar to those reported in previous studies (amplitude:  $70.3 \pm 8.1$  mV; half-width:  $1.2 \pm 0.2$  ms; N=15) (Buckmaster and

Amaral 2001; Hemond et al. 2008). I–V curve showed an outward and inward rectification in the majority of the cells (Fig. 1c). Mean values for  $\tau_m$  and  $R_N$  were  $43 \pm 13.1$  ms and  $148 \pm 69$  M $\Omega$ , respectively (N=25), consistent with previous measurements of the passive properties of CA3 pyramidal cells (Spruston and Johnston 1992; Hemond et al. 2009). The AMPAR- and NMDAR-mediated subthreshold EPSPs/EPSCs (Fig. 1d) had similar kinetics to those reported previously (Debanne et al. 1998; Williams and Johnston 1991; Weisskopf and Nicoll 1995).

### 3.1 Characterization of isolated A/C AMPA uEPSP/uEPSC

CA3 pyramidal cells receive input from other CA3 pyramidal cells via the A/C axons making synaptic contacts onto the apical dendrites in the str. radiatum, and basal dendrites in the str. oriens. A/C synapses on the apical dendrites are positioned throughout the entire str. radiatum (Ishizuka et al. 1990; Li et al. 1994). We took advantage of the widespread dendritic location of A/C synapses to evaluate propagation of synaptic responses along the apical dendrites by comparing the amplitude and kinetic parameters of the isolated AMPA uEPSPs/uEPSCs evoked from various stimulation sites in the str. radiatum (150–300  $\mu$ m from the str. pyramidale) (Fig. 1a, b). Although passive models (Henze et al. 1996; Major et al. 1994; Spruston et al. 1993) predict an attenuation of the responses along the apical dendrite as they travel to the soma, active mechanisms may change the amplitude and kinetics of the synaptic waveform during propagation. Moreover, the A/C axons branch profusely in str. radiatum and extend locally in all directions rather than preferentially parallel to the layer (Li et al. 1994). Thus, the proximal vs. distal site of stimulation in str. radiatum does not necessarily correspond to proximal and distal locations on the apical dendritic tree of the stimulated CA3pc.

Isolated AMPA uEPSPs evoked from proximal, medial, and distal stimulation sites in the str. radiatum (see Section 2) were obtained from 9 neurons (Fig. 3a) at hyperpolarized membrane voltages ( $V_m = -80$  mV) to increase the driving force, and thus the size of the synaptic responses. Figure 3(a) shows EPSPs evoked from proximal and distal str. radiatum and Fig. 3(b) shows the EPSP peak value, TTP, and HHW distributions from one cell, which had CV of 0.47, 0.35, and 0.34, respectively. The variability in amplitude and kinetics was similar across individual cells, with mean CVs of  $0.38 \pm 0.12$ ,  $0.32 \pm 0.11$ , and  $0.34 \pm 0.06$  for PV, TTP, and HHW, respectively. The PV, TTP, and HHW distributions were all fitted with one-peak Gaussian functions (see legend for mean values). We found no significant differences in amplitude and kinetic parameters between AMPA uEPSP evoked from proximal vs. distal radiatum stimulation sites (Supplementary Figure 4). This result is consistent with previous anatomical studies, which showed that A/C fibers follow a non-laminar course forming synapses throughout the whole extent of the apical dendritic tree in str. radiatum (Li et al. 1994).

In light of these results, we attempted a different experimental strategy to distinguish synapses on the proximal vs. distal apical dendrites. In a passive cell, the rise-time of the somatic EPSP/EPSC is affected by the electrotonic distance of the synapse from the soma (Jack et al. 1971), and can be used as an estimator of synapse location. In this case, the rise-time could be a useful index to categorize AMPA uEPSPs as produced from proximal or distal A/C synapses. More generally, a comparison of uEPSP amplitude and kinetics would lend to a full characterization of dendritic propagation. However, it is known that the kinetics of uEPSPs can be modified by the activation of voltage-dependent conductances in a distance-dependent manner (Hoffman et al. 1997; Magee 1998; Williams and Stuart 2000). In this case, the rise-time may not be a helpful index for determining synaptic distance from the soma. Indeed, we found a low correlation between mean HHW and rise-time ( $r < 0.4$ ; Fig. 3c), and between mean uEPSP peak value and rise-time or HHW across cells ( $r < 0.4$ ; Figs. 3d, e). In particular, AMPA uEPSPs generated at different synaptic locations along the

apical and basal dendritic tree appear to have similar mean PV ( $0.3 \pm 0.1$  mV; Table 2). This lack of correlation between mean HHW and rise-time, as well as between mean PV and rise-time or HHW suggests that voltage-dependent conductances may be involved in shaping AMPA uEPSPs.

To prevent the activation of voltage-dependent conductances located close to the soma AMPA uEPSCs ( $N=14$ ;  $V_h = -80$  mV) were evoked from the stimulation sites in the str. radiatum (Fig. 4a). As in the case of CC recordings, there was variability in PV, TTP, and HHW within individual cells illustrated by the corresponding distributions for one cell (Fig. 4b). The variability in amplitude and kinetics was similar across individual cells, with mean CVs of  $0.33 \pm 0.07$ ,  $0.35 \pm 0.14$ , and  $0.29 \pm 0.14$  for PV, TTP, and HHW. Similarly we found no significant differences in amplitude and kinetic parameters between AMPA uEPSC evoked from proximal vs. distal radiatum stimulation sites (Supplementary Figure 5). However, we found high correlations between mean AMPA uEPSC HHW vs. rise-time, mean PV vs. rise-time, and mean PV vs. HHW (Fig. 4c). Because these data are consistent with the effects of dendritic filtering on uEPSCs, rise-time could be used to evaluate synaptic distance from the soma. Based on the mean rise-time from individual cells we identified two groups of AMPA uEPSC: less than 3 ms ( $2.7 \pm 1.2$  ms), and between 3 and 4 ms ( $3.3 \pm 1.3$  ms;  $p < 0.02$ ; Table 3; Fig. 4d, inset). The AMPA uEPSCs with faster mean rise-time had significantly bigger mean PV than those with slower mean rise-time ( $-11.8 \pm 4.8$  pA vs.  $-6.9 \pm 3.7$  pA;  $p < 0.02$ ; Fig. 4d, inset) and shorter mean HHW ( $14.1 \pm 5.7$  ms vs.  $19.7 \pm 7.6$  ms;  $p < 0.05$ ; Fig. 4d, inset; Table 3). Thus, the mean PV and HHW of fast and slow AMPA uEPSCs is in agreement with A/C synapses being located proximally and distally with respect to the soma, respectively. This finding agrees with CA3 passive models (Henze et al. 1996; Major et al. 1994; Spruston et al. 1993), which predict larger and faster synaptic responses from synapses located proximally to the soma. It also suggests that active conductances close to the soma are shaping A/C AMPA uEPSP. These results are further expanded in the companion paper (Baker et al. 2010).

### 3.2 Location-independence of A/C and PPAMPA-mediated uEPSPs

The comparison of EPSP amplitudes and kinetics generated from A/C and PP synapses on the apical dendrite could be helpful for understanding the mechanisms involved in the EPSPs shaping and boosting as they propagate to the soma. Because no correlation was found between mean rise-time and PV for responses evoked by str. radiatum stimulations (Fig. 3d), these data were pooled for the purpose of comparing A/C vs. PP uEPSPs.

Unitary responses from PP were recorded in CC conditions from the same cells in which A/C uEPSP were assessed ( $V_m = -80$  mV;  $N=9$ ; Fig. 5a). Similarly to A/C AMPA uEPSP, there was variability in the trial to trial PV, TTP, and HHW of PP AMPA uEPSPs in individual cells, as shown in corresponding parameter distributions for one cell (Fig. 5b; in gray). As depicted in the cumulative histogram for PV (Fig. 5c), no significant difference in AMPA uEPSP amplitude across all cells was found between A/C and PP ( $0.3 \pm 0.1$  mV and  $0.3 \pm 0.1$  mV;  $p > 0.8$  Fig. 5c, inset; Table 2). The PV histograms from one cell show that A/C and PP responses had similar amplitudes (Fig. 5b) with  $\mu$  obtained from fits of  $0.26 \pm 0.08$  mV and  $0.25 \pm 0.01$  mV for A/C and PP, respectively. As predicted by cable theory, the TTP was significantly slower for PP uEPSPs ( $20.9 \pm 5.7$  ms vs.  $14.8 \pm 5.6$  ms;  $p < 0.001$ ; Fig. 5c). The difference in TTP values between responses from two pathways is evident from the cumulative histograms for all unitary events (Fig. 5c), and the Gaussian fit of TTP distribution for one cell (Fig. 5b;  $16.9 \pm 0.8$  ms vs.  $11.6 \pm 0.18$  ms for PP and A/C, respectively). However, no significant difference in the AMPA uEPSP HHWs was found between A/C and PP ( $40.9 \pm 15.3$  ms, and  $38.0 \pm 13.6$  ms;  $p > 0.05$ ; Fig. 5c, inset; Table 2).

### 3.3 Involvement of voltage-dependent conductances in the shaping of A/C and PP AMPAR-mediated uEPSCs

Theoretical models predict larger and faster somatic responses for A/C than for PP AMPA uEPSPs (Henze et al. 1996; Major et al. 1994; Spruston et al. 1993), but our data show that A/C and PP AMPA uEPSP had comparable amplitudes and durations. As shown above for A/C AMPA uEPSPs, a possible explanation for this result is that VDCs close to the soma shape these responses. To explore this, PP AMPA uEPSCs were recorded from 14 neurons in VC condition (Fig. 6). Similarly to A/C AMPA uEPSC, there was trial-to-trial variability in the PV, TTP, and HHW of PP AMPA uEPSPs within individual cells as shown for the corresponding parameter distributions from one cell (Fig. 6b). However, the variability in PV for PP uEPSC was significantly smaller than for A/C uEPSCs (CV:  $0.20 \pm 0.04$  vs.  $0.33 \pm 0.07$ ;  $p < 0.05$ ).

The neurons from which PP AMPA uEPSCs were recorded are the same in which the two groups of faster and slower A/C AMPA uEPSCs were identified above based on rise-time measurements. Because of that, we compared faster or slower A/C AMPA uEPSCs vs. PP. The faster and slower A/C synapses, are both located proximally to the soma compared to PP synapses, which are in str. lacunosum-moleculare. Thus, we expect A/C AMPA uEPSCs of both subtypes to be larger and faster than those from PP. Firstly; we compared AMPA uEPSCs from faster A/C vs. PP. Representative traces from one cell appear in Fig. 6(a). These faster AMPA uEPSCs from A/C had significantly larger amplitudes than those from PP ( $-11.8 \pm 4.8$  pA vs.  $-6.6 \pm 2.0$  pA;  $p < 0.02$ ; Table 3; Fig. 6c, inset) as shown in the cumulative histogram for PV. Accordingly, the PP AMPA uEPSCs had significantly slower TTP than those of the faster A/C AMPA uEPSPs ( $13.2 \pm 5.6$  ms vs.  $6.1 \pm 2.1$  ms;  $p < 0.001$ ; Table 3; Fig. 6c, inset). The HHW of AMPA uEPSCs also was significantly longer for PP than for faster A/C ( $24.3 \pm 7.1$  ms vs.  $14.1 \pm 5.7$  ms,  $p < 0.001$ ; Table 3; Fig 6c, inset).

Next we compared AMPA uEPSCs from slower A/C vs. PP. Representative traces from one cell in which responses from both pathways were recorded are shown in Fig. 6(a). No significant difference in AMPA uEPSCs peak value was found between distal A/C and PP ( $-6.9 \pm 3.7$  pA vs.  $-6.6 \pm 1.2$  pA;  $p > 0.9$ ; Table 3; Fig. 6d, inset). Nevertheless, as expected for more distal synapses, PP AMPA uEPSCs had significantly slower TTP than those of slower A/C AMPA uEPSCs ( $13.2 \pm 5.6$  ms vs.  $7.7 \pm 3$  ms;  $p < 0.001$ ; Table 3; Fig. 6d, inset) as shown in the cumulative histogram for TTP.

Thus, in contrast to the results obtained in CC condition, the AMPA uEPSCs from A/C synapse with slower rise-time and from PP were smaller and slower than those from A/C synapse with faster rise-time. This is consistent with the involvement of VDCs in boosting A/C and PP AMPA uEPSPs to yield location-independence of somatic amplitudes. These conductances should be close to the soma to be under adequate space clamp control (Spruston et al. 1993; Williams and Mitchell 2008). However, in disagreement with the expectations of larger A/C responses if only passive propagation was involved, no significant differences were found between the AMPA uEPSCs from A/C synapses with slower rise-time (located in distal str. radiatum based on rise time quantification) vs. PP synapses (located more distally in str. lacunosum-moleculare). This suggests that in addition to VDCs close to the soma unclamped VDC located distally from the soma may be also shaping propagation of the synaptic responses. To test this hypothesis, A/C and PP uEPSC were recorded in passive VC conditions (see Section 2; Fig. 7a). The cumulative graph of AMPA uEPSCs recorded from 10 neurons in passive VC condition (Fig. 7b) shows a clear separation in the PV distribution of AMPA uEPSCs between slow A/C (black) and PP (gray). The PVs of slower A/C AMPA uEPSCs were significantly larger ( $-18 \pm 8.1$  pA for A/C vs.  $-9.1 \pm 5.7$  pA, for PP;  $p < 0.05$ ; Table 3). Moreover, as indicated by the significant shift to the right in the PV distribution of responses recorded in VC (black dashed line) vs.

passive VC (black line) ( $p < 0.02$ ), the blockade of active conductances produced an increase in amplitude of distal A/C AMPA uEPSCs (Fig. 7b). This suggests that activation of VDCs located distally from the soma are dampening distal A/C AMPA responses. This effect could explain the similarities in amplitudes between distal A/C and PP responses in VC condition. In the companion paper (Baker et al. 2010), several hypothesis on the possible conductances involved and changes in the axial resistivity were tested. At the same time, the blockade of active conductances did not significantly shift the PV of PP AMPA uEPSCs in VC (gray dashed line) vs. passive VC (gray line) ( $p > 0.1$ ; Fig. 7b). This suggests that unclamped voltage dependent conductances did not significantly affect PP uEPSC amplitudes in the VC condition. This is an arresting finding since PP signals must travel through dendrites in str. radiatum to reach the soma, and are thus expected to be similarly affected by the membrane properties shaping A/C inputs. In the Discussion we hypothesize several plausible mechanisms that could explain this apparent paradox.

In passive VC condition, the TTP of AMPA uEPSCs was significantly slower for PP than A/C ( $10.5 \pm 4.5$  ms vs.  $7.5 \pm 3.2$  ms;  $p < 0.02$ ; Fig. 7b; Table 3). The HHW for PP AMPA uEPSCs also was significantly longer than for A/C ( $19.1 \pm 6.4$  ms vs.  $13.6 \pm 4.1$  ms,  $p < 0.001$ ; Table 3; Fig. 7b). Cumulative graphs also show the expected shift to the right of PP distribution when compared to A/C. Although a trend existed towards faster TTP for PP AMPA uEPSCs in VC (gray dashed line) vs. passive VC (gray line) (Fig. 7b), no significant differences in TTP were found across all cells ( $p > 0.05$ ). Thus, the pharmacological blockade of the active conductances does not significantly affect the kinetic parameters of A/C and PP AMPA uEPSCs, suggesting that the unclamped conductances are not shaping response kinetics. In summary, the peak value was the main parameter shaped by the voltage-dependent conductances. The experiments in VC and in passive VC suggest that conductances both close and distally to the soma are shaping the uEPSP from A/C and PP synapses in CA3 pyramidal cells.

### 3.4 Location-independence of isolated A/C and PP NMDAR-mediated uEPSPs

NMDA uEPSPs were recorded at depolarized membrane voltages ( $V_m = -65$  mV;  $N=8$ ) and in low  $Mg^{2+}$  ( $50 \mu M$ ; Fig. 8a). Although theoretical models predict less dendritic filtering for the slow NMDA synaptic responses, some waveform distortion is still expected (Johnston and Brown 1983; Spruston et al. 1993; Williams and Mitchell 2008; but see Spruston et al. 1995). Consistent with this, HHW and rise-time of A/C and PP NMDA uEPSP were correlated (Fig. 8b;  $r=0.5$  and  $0.3$ , for A/C and PP, respectively). The PV of NMDA uEPSP was moderately correlated with both rise-time and HHW for A/C but not for PP responses (Fig. 8c, d;  $r=0.5$  and  $0.15$ , for A/C and PP, respectively). Similarly to the analysis carried out on AMPA responses, we identified two groups of A/C NMDA uEPSPs based on the mean rise-time from individual cells. One group had significantly faster rise-time ( $12.1 \pm 6.3$  ms) than the other ( $18.2 \pm 7.9$  ms,  $p < 0.05$ ). However, when PV and HHW from both groups were compared we found no significant differences, suggesting a location-independence of A/C NMDA uEPSP amplitudes at the soma.

We further compared the PV, TTP, and HHW between A/C and PP NMDA uEPSP. As shown by the PV, TTP, and HHW histograms corresponding to A/C and PP NMDA uEPSPs recorded from one cell (Fig. 8e), no significant differences were detected (Table 4). In the cell depicted in Fig. 8(e), the mean PV obtained from Gaussian fits was similar for both pathways ( $0.17 \pm 0.01$  mV, and  $0.16 \pm 0.01$  mV for A/C and PP, respectively). Interestingly, the TTP histogram for A/C NMDA uEPSP was fitted with two Gaussian peaks ( $27.0 \pm 1.2$  ms, and  $46.8 \pm 2.5$  ms), whereas the TTP histogram for PP NMDA uEPSP was fitted with a one-peak Gaussian ( $38.7 \pm 1.9$  ms). As shown in the TTP histogram, the stimulation of both pathways evoked responses with fast and slow kinetic in the same cell (Fig. 8e). The most plausible explanation for this finding is that minimal stimulation reliably evoked responses

from two different fibers with different electrotonic distance from the soma. The activation of PP synapses also showed variability in the mean rise-time among cells, with some cells displaying faster mean rise-time than others, but these differences were not significant (data not shown). As in the case of AMPA uEPSP/uEPSC, there was variability in PV, TTP, and HHW of A/C and PP NMDA uEPSPs within individual cells as shown in the distributions for one cell (Fig. 8e). The CV of peak values was significantly smaller for PP than for A/C NMDA uEPSP ( $0.25 \pm 0.05$  vs.  $0.36 \pm 0.14$ ;  $p < 0.05$ ).

Because synapses in str. lacunosum-moleculare are the most distally located in the apical dendrites of CA3 pyramidal cells, PP NMDA uEPSP are expected to be more filtered and attenuated than A/C NMDA uEPSP. However, as for AMPA uEPSPs/uEPSCs, mechanisms such as shaping by voltage-dependent conductances (Fernandez de Sevilla et al. 2007; Ngo-Anh et al. 2005; Otmakhova and Lisman 2004) could be responsible for the location-independence at the soma of NMDA uEPSP responses from A/C and PP. To explore this possibility, we recorded NMDA-mediated unitary responses from both pathways in VC and passive VC conditions.

### 3.5 Active processes are not involved in the propagation of A/C and PP NMDAR-mediated uEPSCs

NMDA uEPSCs from both pathways were recorded in VC and passive VC conditions in 12 and 10 neurons, respectively (Fig. 9a, b). As in the CC condition, we identified two groups of A/C NMDA uEPSC in the VC and passive VC condition based on mean rise-time from individual cells: one with faster ( $9.5 \pm 5.9$  ms and  $8.3 \pm 5.6$  ms), and other with slower rise-time ( $12.7 \pm 7.3$  ms and  $11.9 \pm 7.1$  ms;  $p < 0.02$ ). However, no significant differences were found in PV and HHW between these groups (data not shown). Interestingly, like in CC condition the activation of PP synapses also showed differences in the mean rise-time among cells in VC and in passive VC condition, with some cells displaying faster mean rise-time than others. However, although a trend existed, the difference between groups was not significant. Interestingly, the CV of PV was significantly smaller for A/C and PP NMDA uEPSC than for A/C and PP NMDA uEPSP ( $0.18 \pm 0.04$  vs.  $0.36 \pm 0.14$ ,  $p < 0.02$ ; and  $0.16 \pm 0.07$  vs.  $0.25 \pm 0.05$ ,  $p < 0.05$ ; for A/C and PP, respectively). The CV of TTP and HHW were similar both between pathways and between recordings conditions (CC vs. VC; data not shown).

The cumulative distribution graph from unitary sweeps across all cells shows a shift towards larger PV for NMDA uEPSCs from PP when compared to those of A/C (Fig. 9c; gray vs. black dashed lines). However, when unitary responses from A/C and PP were compared across all cells, no significant difference was found ( $-4.5 \pm 1.7$  pA vs.  $-3.8 \pm 1.7$  pA;  $p > 0.6$ ; Table 4). Cumulative distributions of TTP and HHW across all cells were similar for A/C and PP uEPSC (Fig. 9c; gray vs. black dashed lines), and no significant differences were found (TTP:  $22 \pm 11$  ms and  $23.8 \pm 11.2$  ms; HHW:  $41.3 \pm 17.5$  ms and  $41.4 \pm 19.0$  ms;  $p > 0.07$ ; Table 4).

Blockade of active conductances in the passive VC condition did not change the outcome obtained in the VC condition (Fig. 9c; black vs. gray lines). The PV, TTP, and HHW distributions from one cell are depicted in Fig. 9(d). The PV of A/C and PP NMDA uEPSP were comparable ( $\mu$ :  $-3.34 \pm 0.07$  pA and  $-3.17 \pm 0.08$  pA, for A/C and PP, respectively). The PV of NMDA uEPSCs across all cells agrees with these results, revealing no significant differences between A/C and PP NMDA uEPSCs ( $-3.5 \pm 1.0$  pA, vs.  $-3.5 \pm 0.8$  pA,  $p > 0.2$ ; Table 4). With respect to kinetic parameters, block of active conductances in the passive VC showed a trend for A/C NMDA uEPSCs towards faster and shorter responses than those from PP (Fig. 9c; black vs. gray line). However, no significant differences in TTP and HHW of NMDA uEPSCs were found across all cells (TTP:  $16.0 \pm 7.7$  ms vs.  $21.8 \pm 12.0$  ms, and

HHW:  $28.6 \pm 10.8$  ms vs.  $37.7 \pm 17.0$  ms; for A/C and PP, respectively; Table 4). The TTP histograms for A/C and PP NMDA uEPSP from one cell (Fig. 9d) were each fitted with two Gaussian peaks (A/C:  $12.6 \pm 0.15$  ms and  $25.3 \pm 2.5$  ms; PP:  $18.04 \pm 0.5$  ms and  $36.3 \pm 3.4$  ms). The histogram mean HHWs in the same cell ( $29.0 \pm 0.6$  ms vs.  $39.8 \pm 1.65$  ms for A/C and PP, respectively) agree with mean HHWs values from all unitary sweeps across all cells. Moreover, no significant differences were found between A/C NMDA uEPSC recorded in VC and passive VC at either  $V_m = -65$  or  $-80$  mV (Supplementary Figure 6). In conclusion, the dendritic propagation of NMDA uEPSP does not seem to be affected by voltage-dependent mechanisms. However, we cannot rule out the possibility that synaptic scaling (Andrasfalvy and Mody 2006; Jansek and Redman 1973; Magee and Cook 2000) or passive normalization (Chitwood et al. 1999; Jaffe and Carnevale 1999) may be involved. These issues are further investigated in the companion paper.

## 4 Discussion

To the best of our knowledge this is the first study in which somatic A/C and PP AMPA and NMDA uEPSP/uEPSC from CA3 pyramidal cells were recorded in active and passive conditions. Furthermore, the experimental data under passive conditions were used to construct a realistic model of passive propagation of responses in the CA3b pyramidal cell, which is described in the companion paper. Thus combination of experimentally somatic recordings with a computational model was used as an indirect method to study dendritic synaptic responses which otherwise would be not possible due to the unfeasibility of recordings from distal dendrites. The comparative analysis of the amplitude and kinetic parameters of A/C and PP somatic uEPSP/uEPSC in different experimental conditions allowed us to draw some conclusions about active and passive mechanisms that may shape the propagation of those synaptic responses. Our results demonstrate location-independence of AMPA and NMDA uEPSP somatic amplitudes for A/C input evoked from str. radiatum (both proximal and distal stimulation sites), and for the PP input evoked from str. lacunosum-moleculare in area CA1. In contrast, larger AMPA uEPSCs were evoked from A/C synapses with faster rise-time than from A/C synapses with lower rise-time or PP, as predicted by the passive model of dendritic propagation described in the companion paper (Baker et al. 2010). Given the space-clamp constraints in pyramidal cells, these VC data suggest that the location-independence of A/C and PP AMPA uEPSP amplitudes is achieved, in part, through the activation of voltage dependent conductances at or near the soma. At the same time, the similar peak value distributions of uEPSCs between slower A/C vs. PP inputs point to the additional participation of active conductances located at distal dendritic sites. Consistent with this idea, the pharmacological blockade of voltage-dependent conductances eliminated the location-independence, and somatic uEPSC from A/C were considerably larger in passive VC than in VC. Together, these findings imply that the amplitude independence of the A/C AMPA inputs with slower rise-time results from dendritic dampening by active conductances. In contrast, the propagation of NMDA uEPSPs was not affected by voltage-dependent mechanisms. Moreover, the rapid decay of A/C and PP NMDA uEPSP/uEPSC were consistent with responses mediated by NR2A receptor subtype, a finding that is further elaborated in the companion paper.

### 4.1 AMPA-mediated unitary responses in CA3 pyramidal neurons

To the best of our knowledge, this is the first detailed characterization of the amplitude and kinetics of pharmacologically isolated A/C and PP AMPA uEPSPs/EPSC in CA3 pyramidal cells. The average A/C AMPA uEPSP peak value in this study is smaller than previously reported (Miles and Wong 1986). One possible reason for this difference is our ability to resolve smaller uEPSP amplitudes reliably (0.1 mV vs. 0.4 mV in the prior study). Although minimal stimulation does not guarantee the activation of single fibers (Dobrunz et al. 1997; Raastad 1995), the small AMPA responses indicate that very few synapses were being

activated in the present study. Moreover, a post-hoc analysis of our unitary selection method, described in the companion paper (Baker et al. 2010) revealed that the estimation bias, i.e. difference between estimated and actual mean, was small and minimally affected by the number of sweeps. Our TTP values of A/C AMPA uEPSPs were similar to those obtained by Sokolov and co-workers (2003) but slower than those in Miles and Wong (1986). A/C synapses have a widespread dendritic location throughout the apical and basal trees in str. radiatum and str. oriens, respectively (Ishizuka et al. 1990; Li et al. 1994). This anatomical organization is consistent with the wide rise-time distributions obtained in the present study for unitary responses evoked from str. radiatum. Therefore, the variability in TTP values among different studies could be due to differences in the proportion of synapses activated on distal vs. proximal dendritic locations.

#### 4.2 Location independence of AMPA uEPSP somatic amplitudes

The present results in CC conditions do not agree with the observations derived from passive models of CA3 pyramidal neurons (Henze et al. 1996; Major et al. 1994; Spruston et al. 1993), which predict larger and faster responses from synapses located proximally. However, location-independence of AMPA EPSPs has been shown in CA1 pyramidal neurons, neocortical neurons, and spinal motoneurons (Andrasfalvy and Mody 2006; Iasek and Redman 1973; Magee and Cook 2000; Nevian et al. 2007). Several studies have shown that activation of voltage-dependent conductances could amplify the EPSPs and thus compensate for their attenuation (Magee and Johnston 1995; Stuart and Sakmann 1995; cf. Johnston and Narayanan 2008; Williams and Stuart 2003). Although the identification of the specific conductances involved in the shaping of EPSPs was beyond the scope of this study, our data address the issue of whether active mechanisms are implicated in the location-independence of AMPA uEPSPs. We found no significant differences in amplitudes of A/C AMPAR uEPSP evoked from proximal vs. distal radiatum or between A/C and PP inputs. However, our experiments in voltage clamp showing that A/C AMPA uEPSCs with faster rise-time were larger than those with slower rise time as well as than PP AMPA uEPSCs point out to the involvement of active processes in shaping AMPA uEPSPs. Because voltage control decreases within short distances from the soma (Johnston and Brown 1983; Spruston et al. 1993; Williams and Mitchell 2008) (see also companion paper: Baker et al. 2010), the conductances involved in the shaping of uEPSPs are probably located near the CA3pc soma. Furthermore, distal conductances might be also involved because the location-independence of EPSCs from slower A/C and PP was eliminated with passive voltage clamp (pharmacological block of the voltage dependent conductances in voltage clamp conditions). The increase in somatic A/C AMPA uEPSCs amplitudes in passive VC vs. VC suggests that the location-independence of EPSCs from slower A/C and PP was likely achieved through the dampening of distal A/C AMPA uEPSCs. Even though our results demonstrate that A/C synaptic responses are strongly affected by voltage-dependent conductances, the effect is much less pronounced in PP synapses, located more distally in str. lacunosum-moleculare. At first this may seem counterintuitive given that apical dendrites receive synaptic contacts with both A/C and PP. Since PP signals must travel through dendrites in str. radiatum to reach the soma, any conductance shaping A/C inputs might be expected to have a similar effect on PP synaptic responses. However, a closer inspection of digital reconstructions of CA3pc dendrites provides a simple explanation for this apparent paradox. Of the dendritic branches innervated by A/C synaptic contacts, only a limited portion of those in str. radiatum, and none of those in str. oriens, extend into str. lacunosum-moleculare. In particular, in the 17 CA3pc morphologies available in the public database NeuroMorpho.Org (Halavi et al. 2008) and used in the modeling study presented in the companion paper, only 19% (by length) of the dendrites potentially receiving A/C input project into str. lacunosum-moleculare where they could receive PP synaptic contacts. In addition, the dendritic branches that continue into LM have on average a larger diameter in

SR than those that do not (0.8 and 0.2  $\mu\text{m}$ , respectively). Differences in ion channel distributions among these two groups of branches as well as differences in local depolarization resulting from synaptic stimulation could account for the different effects of voltage-dependent conductances on PP and A/C synaptic responses. For instance, a lower density of  $K_A$  in str. radiatum in the small proportion of larger dendrites projecting to str. lacunosum-moleculare would explain the lack of attenuation from PP synapses without substantially altering the strong effect observed in A/C synapses.

Yet another possibility is the presence of SK potassium channels co-located with  $\text{CaV}_{2,3}$  calcium channels in spines. In CA1 pyramidal cells at 33°, but not at room temperature, this pairing of active channels reduced uEPSPs approximately two-fold (Bloodgood and Sabatini 2007), similar to the differences found here between VC and passive VC in uEPSCs. Channels located on spines would more effectively shape local synaptic inputs than signals traveling in the underlying dendritic shafts. Thus, conductances expressed in str. radiatum spines could explain the stronger attenuation of A/C vs. PP responses (see companion paper: Baker et al. 2010). Furthermore, excitatory synapses in str. lacunosum-moleculare have fewer spines than in the rest of the dendritic trees (Ishizuka et al. 1995) and thus may be less affected by channels found primarily in spines.

### 4.3 NMDA-mediated unitary responses in CA3 pyramidal neurons

The peak value and TTP from A/C NMDA uEPSP are close to the values reported previously for unitary connections between CA3 pyramidal neurons in slice cultures (Debanne et al. 1998). To the best of our knowledge, however, this is the first characterization of NMDAR-mediated unitary responses on CA3 pyramidal neurons in slices from adult animals. We found that NMDA uEPSCs from A/C and PP have faster decay time than in parasympathetic neurons (Araki and de Groat 1996), but similar for unitary connections between pairs of excitatory L4 spiny neurons from somatosensory cortex (Feldmeyer et al. 2002). Dendritic filtering could affect the kinetic of NMDA uEPSPs/uEPSCs in a distance-dependent manner. Thus, it is necessary to be cautious when the kinetics from different inputs is compared within the same neuron as well as across different types of neurons. Nonetheless, it is well known that kinetic properties of NMDA EPSC/EPSP depend on the subunit composition of the channel receptor complex. NR1/NR2A receptors endow NMDA EPSC with faster kinetic than NR1/NR2B receptors (Chen et al. 1999; Vicini et al. 1998). In hippocampal pyramidal cells, NR1, NR2A and NR2B subunits are highly expressed (Monyer et al. 1994; Moriyoshi et al. 1991). Studies using ifenprodil have shown that the majority of NMDA receptors in the A/C CA3 synapse are composed mainly of NR1/NR2A subunits (Ito et al. 2000). Furthermore, the fast decay kinetic of A/C and PP NMDA uEPSP/uEPSC suggest that NMDAR in these synapses are mainly composed of NR1/NR2A subunits. Hence, simulations of our experimental data using a passive model, described in the companion paper (Baker et al. 2010) show that responses from NMDAR synapses are best fit by assuming rapid NMDA receptor kinetic indicative of NR2A receptor subunit. Although ifenprodil effects have not been tested in PP synapses on CA3 pyramidal cells, experiments in CA1 pyramidal and granular cells have shown sensitivity to this drug (Arrigoni and Greene 2004) suggesting the presence of NR2B subunits. Our data showed no differences in the kinetic of A/C vs. PP NMDA uEPSPs/uEPSCs at the soma. Because A/C and PP uEPSPs/uEPSCs are subject to different degree of filtering, their kinetic is probably different at the synaptic sites. Moreover, the dendritic morphology could also determine the kinetics of the NMDA uEPSP. For example, because of lower local capacitance the kinetics would be faster in thinner distal dendrites than in thicker dendrites (Williams and Stuart 2003).

#### 4.4 Location independence of NMDAR-mediated uEPSP/uEPSC amplitudes in the soma

Despite the importance of NMDAR in plasticity and synaptic integration, only few studies have addressed the propagation of NMDA EPSP/EPSC (Arrigoni and Greene 2004; Fernandez de Sevilla et al. 2007). Nevertheless, it has been shown that NMDA EPSP/EPSC could be shaped by voltage-dependent conductances (Fernandez de Sevilla et al. 2007; Ngo-Anh et al. 2005; Otmakhova and Lisman 2004).

In our experimental conditions, voltage-dependent conductances do not seem to be involved in the regulation of NMDA uEPSP/uEPSC. The most plausible explanation for this result is that fast activation/inactivation times of dendritic voltage-dependent conductance involved may affect only the AMPA uEPSP/uEPSC. For example, the transient  $K^+$  current, which has fast activation and inactivation time constants (Mitterdorfer and Bean 2002), might affect fast AMPAR but not slow NMDAR responses. However, it cannot be assumed that all voltage-dependent conductances that could affect the dendritic propagation of AMPA and NMDA uEPSP/uEPSC were blocked since specific blockers were not used for all of them.

If voltage-dependent conductances are not involved in shaping NMDA uEPSP/uEPSC, then similar amplitudes of A/C vs. PP responses could be due to passive normalization (Chitwood et al. 1999; Jaffe and Carnevale 1999). Specifically, the combination of electronically short dendrites in CA3 pyramidal cells with specific branching pattern may lead to location independence of transfer impedance (Jaffe and Carnevale 1999). Accordingly, the anatomic and “passive” biophysical properties of the cell coalesce to remove most of the dependence of somatic EPSP amplitude on synaptic location. The quantitative analysis of simulations carried out with the computational model described in the companion paper (Baker et al. 2010) suggests numerically that location independence of NMDA uEPSP/uEPSC may be explained by passive normalization combined with a marginal amount of differential scaling between pathways (~12% difference in synaptic conductance between A/C and PP).

#### 4.5 Comparison between pyramidal CA1 and CA3 pyramidal cells

Although CA3 and CA1 pyramidal neurons have some common properties (e.g. two dendritic fields (basilar and apical)), they have different electrotonic architectures. Specifically CA1 pyramidal cells generally have a single primary apical dendrite whereas CA3 have multiple apical branches. This anatomical difference produces a larger passive attenuation along CA1 pyramidal cells apical dendrites than in CA3 pyramidal cells (Jaffe and Carnevale 1999). CA1 pyramidal cells are endowed with several compensatory mechanisms for this passive attenuation, including distance-dependent scaling of uEPSP from Schaffer collateral axons (Andrasfalvy and Magee 2001; Magee and Cook 2000; Nicholson et al. 2006; Smith et al. 2003). However, in CA3 pyramidal cells simulations of our experimental data from passive VC (see companion paper) indicate that synaptic scaling is unlikely to be responsible for the location-independence of AMPA uEPSP amplitudes (Baker et al. 2010). As discussed previously, in CA3 pyramidal cells the activation of VDCs is the main mechanism to compensate for passive attenuation. In contrast, active mechanisms present in the CA1 pyramidal neurons (Magee and Johnston 1995) seem to play a minor role (Magee and Cook 2000) as a compensatory mechanism.

In the present work, we found no significant differences between A/C and PP NMDA uEPSP/uEPSC across all recording conditions in CA3 pyramidal cells. This result stands in stark contrast with studies in CA1 pyramidal cells that reported larger NMDA subthreshold EPSCs for PP input than for Schaffer collateral axons (Otmakhova et al. 2002; Arrigoni and Greene 2004). In agreement with our data, however, these studies showed that the voltage-dependent conductances were not responsible for differences in amplitude between

pathways (Arrigoni and Greene 2004; Otmakhova et al. 2002). In CA1 pyramidal neurons, there is no evidence of synaptic scaling for the NMDA receptors (Andrasfalvy and Magee 2001; Nicholson et al. 2006; Smith et al. 2003). Nevertheless, this mechanism should not be ruled out as responsible for the location-independence of amplitudes in CA3 pyramidal cells since differences in NMDA receptor subunits have been reported between both cell types (Coultrap et al. 2005; Spruston et al. 1995).

#### 4.6 Functional implications

Hippocampal area CA3 is critically involved in the encoding of new contextual memories, spatial working memory, and in spatial pattern separation (cf. Kesner 2007; Leutgeb et al. 2007; Rolls 2007). According to computational studies, the mnemonic function of area CA3 is subserved by its unique connectivity features such as the autoassociative network formed by the A/C connections among pyramidal cells (Kesner 2007; Rolls 2007). Indeed, each CA3pc receives several thousand inputs from other CA3 pyramidal cells (Wittner and Miles 2007). Furthermore, behavioral and computational studies attribute an important role to PP input in strengthening A/C synapses on CA3 pyramidal cells, as shown in the intact preparation (Martinez et al. 2002). The present results also are consistent with the idea that despite its most distal dendritic location, the PP input represents a significant input to CA3 pyramidal cells (Yeckel and Berger 1990; Urban et al. 1998). The independence of somatic response amplitude to the dendritic location reported here would allow inputs from A/C and PP to influence equally the precision of EPSP-spike coupling (Ascoli 2003). Moreover, the location-independence for proximal and distal A/C synapses could be important during synchronized activation of the network during gamma oscillations (Oren et al. 2006), disinhibition induced synchrony (de la Prida et al. 2006; Wittner and Miles 2007), and sharp waves (Csicsvari et al. 2000). The threshold to initiate synchronous population bursts depends on the recruitment of CA3 pyramidal cells via recurrent collateral connections (de la Prida et al. 2006; Traub and Wong 1982). At the beginning of the build-up period, only small numbers of CA3 pyramidal cells may be active, and thus less recurrent excitatory inputs may be available to recruit other CA3 pyramidal cells (de la Prida et al. 2006). In this case, activation of few A/C proximal or distal synapses would have the same impact at the soma, decreasing the number of CA3 pyramidal cells necessary to initiate to recruit additional CA3 pyramidal cells.

The location-independence of somatic EPSPs is probably one of the ways in which distal PP inputs would impact the neuron output at the soma. In CA1 pyramidal neurons, both the generation of distal dendrites spikes (Jarsky et al. 2005) and the potentiation of Schaffer collaterals axons by PP stimulation (Dudman et al. 2007) influence somatic spiking. Because CA3 pyramidal cells may also support dendritic spike initiation (Lazarewicz et al. 2002; Wong et al. 1979), NMDA receptors at A/C synapses could enable a similar input time-depending plasticity induced by activation of PP (Dudman et al. 2007). Thus, our study suggest that like other pyramidal neurons (Magee and Cook 2000; Nevian et al. 2007), the CA3 pyramidal cell is also endowed with active and passive mechanisms to modulate the propagation of synaptic responses.

#### Supplementary Material

Refer to Web version on PubMed Central for supplementary material.

#### Acknowledgments

This work was supported by NIH Grants AG025633, NS39600, and NS24288. We thank John Cavaretta for technical assistance and Warren Anderson for help in some steps of the analysis.

## Abbreviations

<b>ACSF</b>	Artificial cerebrospinal fluid
<b>AMPA and NMDA uEPSP/uEPSC</b>	AMPA and NMDA receptor-mediated unitary EPSP/EPSC
<b>A/C</b>	Associational/commissural
<b>AR</b>	Adaptation ratio
<b>CC</b>	Current clamp
<b>CNQX</b>	6-cyano-7-nitroquinoxaline-2, 3-dione
<b>CV</b>	Coefficient of variation
<b>D-APV</b>	D(-)-2-amino-5-phosphonopentanoic acid
<b>DIC</b>	Differential interference contrast
<b>EC</b>	Entorhinal cortex
<b>HHW</b>	Half-height width
<b><math>I_h</math></b>	Hyperpolarization-activated current
<b><math>K_A</math></b>	A-type potassium ion channels
<b>MF</b>	Mossy fiber
<b>PP</b>	Perforant-path
<b>PV</b>	Peak value
<b><math>R_N</math></b>	Input resistance
<b>str.</b>	Stratum
<b>TTP</b>	Time-to-peak
<b>VC</b>	Voltage clamp
<b>VDC</b>	Voltage-dependent conductances
<b><math>V_m</math></b>	Membrane voltage
<b><math>V_h</math></b>	Holding membrane voltage
<b><math>\mu</math></b>	Mean Gaussian value
<b><math>\tau_m</math></b>	Membrane time constant

## References

- Andrasfalvy BK, Magee JC. Distance-dependent increase in AMPA receptor number in the dendrites of adult hippocampal CA1 pyramidal neurons. *The Journal of Neuroscience*. 2001; 21:9151–9159. [PubMed: 11717348]
- Andrasfalvy BK, Mody I. Differences between the scaling of miniature IPSCs and EPSCs recorded in the dendrites of CA1 mouse pyramidal neurons. *Journal de Physiologie*. 2006; 576:191–196.
- Araki I, De Groat WC. Unitary excitatory synaptic currents in preganglionic neurons mediated by two distinct groups of interneurons in neonatal rat sacral parasympathetic nucleus. *Journal of Neurophysiology*. 1996; 76:215–226. [PubMed: 8836220]
- Arrigoni E, Greene RW. Schaffer collateral and perforant path inputs activate different subtypes of NMDA receptors on the same CA1 pyramidal cell. *British Journal of Pharmacology*. 2004; 142:317–322. [PubMed: 15155538]

- Ascoli GA. Passive dendritic integration heavily affects spiking dynamics of recurrent networks. *Neural Networks*. 2003; 16:657–663. [PubMed: 12850020]
- Baker JL, Perez-Rosello T, Migliore M, Barrionuevo G, Ascoli GA. A computer model of unitary responses from associational/commissural and perforant path synapses in hippocampal CA3 pyramidal cells. *J Comput Neurosci*. 2010
- Berzhanskaya J, Urban NN, Barrionuevo G. Electrophysiological and pharmacological characterization of the direct perforant path input to hippocampal area CA3. *Journal of Neurophysiology*. 1998; 79:2111–2118. [PubMed: 9535972]
- Blackstad TW, Brink K, Hem J, Jeune B. Distribution of hippocampal mossy fibers in the rat. An experimental study with silver impregnation methods. *The Journal of Comparative Neurology*. 1970; 138:433–449. [PubMed: 4907846]
- Bloodgood BL, Sabatini BL. Nonlinear regulation of unitary synaptic signals by CaV<sub>2,3</sub> voltage-sensitive calcium channels located in dendritic spines. *Neuron*. 2007; 53:249–260. [PubMed: 17224406]
- Buckmaster PS, Amaral DG. Intracellular recording and labeling of mossy cells and proximal CA3 pyramidal cells in macaque monkeys. *The Journal of Comparative Neurology*. 2001; 430:264–281. [PubMed: 11135261]
- Chen N, Luo T, Raymond LA. Subtype-dependence of NMDA receptor channel open probability. *The Journal of Neuroscience*. 1999; 19:6844–6854. [PubMed: 10436042]
- Chitwood RA, Hubbard A, Jaffe DB. Passive electrotonic properties of rat hippocampal CA3 interneurons. *Journal de Physiologie*. 1999; 515:743–756.
- Claiborne BJ, Amaral DG, Cowan WM. A light and electron microscopic analysis of the mossy fibers of the rat dentate gyrus. *The Journal of Comparative Neurology*. 1986; 246:435–458. [PubMed: 3700723]
- Coultrap SJ, Nixon KM, Alvestad RM, Valenzuela CF, Browning MD. Differential expression of NMDA receptor subunits and splice variants among the CA1, CA3 and dentate gyrus of the adult rat. *Brain Research Molecular Brain Research*. 2005; 135:104–111. [PubMed: 15857673]
- Csicsvari J, Hirase H, Mamiya A, Buzsaki G. Ensemble patterns of hippocampal CA3-CA1 neurons during sharp wave-associated population events. *Neuron*. 2000; 28:585–594. [PubMed: 11144366]
- de la Prida LM, Huberfeld G, Cohen I, Miles R. Threshold behavior in the initiation of hippocampal population bursts. *Neuron*. 2006; 49:131–142. [PubMed: 16387645]
- Debanne D, Gähwiler BH, Thompson SM. Long-term synaptic plasticity between pairs of individual CA3 pyramidal cells in rat hippocampal slice cultures. *Journal de Physiologie*. 1998; 507:237–247.
- R Development Core Team. R: A language and environment for statistical computing. R Foundation for Statistical Computing; Vienna, Austria: 2008. URL <http://www.R-project.org>
- Dobrunz LE, Huang EP, Stevens CF. Very short-term plasticity in hippocampal synapses. *Proceedings of the National Academy of Sciences of the United States of America*. 1997; 94:14843–14847. [PubMed: 9405701]
- Dudman JT, Tsay D, Siegelbaum SA. A role for synaptic inputs at distal dendrites: instructive signals for hippocampal long-term plasticity. *Neuron*. 2007; 56:866–879. [PubMed: 18054862]
- Feldmeyer D, Lubke J, Silver RA, Sakmann B. Synaptic connections between layer 4 spiny neurone-layer 2/3 pyramidal cell pairs in juvenile rat barrel cortex: physiology and anatomy of interlaminar signalling within a cortical column. *Journal de Physiologie*. 2002; 538:803–822.
- Fernandez de Sevilla D, Fuenzalida M, Porto Pazos AB, Buno W. Selective shunting of the NMDA EPSP component by the slow afterhyperpolarization in rat CA1 pyramidal neurons. *Journal of Neurophysiology*. 2007; 97:3242–3255. [PubMed: 17329628]
- Halavi M, Polavaram S, Donohue DE, Hamilton G, Hoyt J, Smith KP, et al. NeuroMorpho.Org implementation of digital neuroscience: dense coverage and integration with the NIF. *Neuroinformatics*. 2008; 6:241–252. [PubMed: 18949582]
- Hemond P, Epstein D, Boley A, Migliore M, Ascoli GA, Jaffe DB. Distinct classes of pyramidal cells exhibit mutually exclusive firing patterns in hippocampal area CA3b. *Hippocampus*. 2008; 18:411–424. [PubMed: 18189311]

- Hemond P, Migliore M, Ascoli GA, Jaffe DB. The membrane response of hippocampal CA3b pyramidal neurons near rest: heterogeneity of passive properties and the contribution of hyperpolarization-activated currents. *Neuroscience*. 2009; 160:359–370. [PubMed: 19232379]
- Henze DA, Cameron WE, Barrionuevo G. Dendritic morphology and its effects on the amplitude and rise-time of synaptic signals in hippocampal CA3 pyramidal cells. *The Journal of Comparative Neurology*. 1996; 369:331–344. [PubMed: 8743416]
- Hoffman DA, Magee JC, Colbert CM, Johnston D. K<sup>+</sup>channel regulation of signal propagation in dendrites of hippocampal pyramidal neurons. *Nature*. 1997; 387:869–875. [PubMed: 9202119]
- Iansek R, Redman SJ. The amplitude, time course and charge of unitary excitatory post-synaptic potentials evoked in spinal motoneurone dendrites. *Journal de Physiologie*. 1973; 234:665–688.
- Ishizuka N, Cowan M, Amaral DG. A quantitative analysis of the dendritic organization of pyramidal cell in the rat hippocampus. *The Journal of Comparative Neurology*. 1995; 362:17–45. [PubMed: 8576427]
- Ishizuka N, Weber J, Amaral DG. Organization of intrahippocampal projections originating from CA3 pyramidal cells in the rat. *The Journal of Comparative Neurology*. 1990; 295:580–623. [PubMed: 2358523]
- Ito I, Kawakami R, Sakimura K, Mishina M, Sugiyama H. Input-specific targeting of NMDA receptor subtypes at mouse hippocampal CA3 pyramidal neuron synapses. *Neuropharmacology*. 2000; 39:943–951. [PubMed: 10727704]
- Jack JJ, Miller S, Porter R, Redman SJ. The time course of minimal excitatory post-synaptic potentials evoked in spinal motoneurons by group Ia afferent fibres. *Journal de Physiologie*. 1971; 215:353–380.
- Jaffe DB, Carnevale NT. Passive normalization of synaptic integration influenced by dendritic architecture. *Journal of Neurophysiology*. 1999; 82:3268–3285. [PubMed: 10601459]
- Jarsky T, Roxin A, Kath WL, Spruston N. Conditional dendritic spike propagation following distal synaptic activation of hippocampal CA1 pyramidal neurons. *Nature Neuroscience*. 2005; 8:1667–1676.
- Johnston D, Brown TH. Interpretation of voltage-clamp measurements in hippocampal neurons. *Journal of Neurophysiology*. 1983; 50:464–486. [PubMed: 6310063]
- Johnston D, Narayanan R. Active dendrites: colorful wings of the mysterious butterflies. *Trends in Neurosciences*. 2008; 31:309–316. [PubMed: 18471907]
- Jonas P, Major G, Sakmann B. Quantal components of unitary EPSCs at the mossy fibre synapse on CA3 pyramidal cells of rat hippocampus. *Journal de Physiologie*. 1993; 472:615–663.
- Kesner RP. Behavioral functions of the CA3 subregion of the hippocampus. *Learning & Memory*. 2007; 14:771–781. [PubMed: 18007020]
- Lawrence JJ, Grinspan ZM, McBain CJ. Quantal transmission at mossy fibre targets in the CA3 region of the rat hippocampus. *Journal de Physiologie*. 2004; 554:175–193.
- Lazarewicz MT, Migliore M, Ascoli GA. A new bursting model of CA3 pyramidal cell physiology suggests multiple locations for spike initiation. *Biosystems*. 2002; 67:129–137. [PubMed: 12459292]
- Leutgeb JK, Leutgeb S, Moser MB, Moser EI. Pattern separation in the dentate gyrus and CA3 of the hippocampus. *Science*. 2007; 315:961–966. [PubMed: 17303747]
- Li XG, Somogyi P, Ylinen A, Buzsaki G. The hippocampal CA3 network: an *in vivo* intracellular labeling study. *The Journal of Comparative Neurology*. 1994; 339:181–208. [PubMed: 8300905]
- Magee JC. Dendritic hyperpolarization-activated currents modify the integrative properties of hippocampal CA1 pyramidal neurons. *The Journal of Neuroscience*. 1998; 18:7613–7624. [PubMed: 9742133]
- Magee JC, Cook EP. Somatic EPSP amplitude is independent of synapse location in hippocampal pyramidal neurons. *Nature Neuroscience*. 2000; 3:895–903.
- Magee JC, Johnston D. Synaptic activation of voltage-gated channels in the dendrites of hippocampal pyramidal neurons. *Science*. 1995; 268:301–304. [PubMed: 7716525]
- Major G, Larkman AU, Jonas P, Sakmann B, Jack JJ. Detailed passive cable models of whole-cell recorded CA3 pyramidal neurons in rat hippocampal slices. *The Journal of Neuroscience*. 1994; 14:4613–4638. [PubMed: 8046439]

- Martinez CO, Do VH, Martinez JL Jr, Derrick BE. Associative long-term potentiation (LTP) among extrinsic afferents of the hippocampal CA3 region *in vivo*. *Brain Research*. 2002; 940:86–94. [PubMed: 12020879]
- McBain C, Dingledine R. Dual-component miniature excitatory synaptic currents in rat hippocampal CA3 pyramidal neurons. *Journal of Neurophysiology*. 1992; 68:16–27. [PubMed: 1355525]
- Miles R, Wong RK. Excitatory synaptic interactions between CA3 neurones in the guinea-pig hippocampus. *Journal de Physiologie*. 1986; 373:397–418.
- Mitterdorfer J, Bean BP. Potassium currents during the action potential of hippocampal CA3 neurons. *The Journal of Neuroscience*. 2002; 22:10106–10115. [PubMed: 12451111]
- Monyer H, Burnashev N, Laurie DJ, Sakmann B, Seeburg PH. Developmental and regional expression in the rat brain and functional properties of four NMDA receptors. *Neuron*. 1994; 12:529–540. [PubMed: 7512349]
- Moriyoshi K, Masu M, Ishii T, Shigemoto R, Mizuno N, Nakanishi S. Molecular cloning and characterization of the rat NMDA receptor. *Nature*. 1991; 354:31–37. [PubMed: 1834949]
- Nevian T, Larkum ME, Polsky A, Schiller J. Properties of basal dendrites of layer 5 pyramidal neurons: a direct patch-clamp recording study. *Nature Neuroscience*. 2007; 10:206–214.
- Ngo-Anh TJ, Bloodgood BL, Lin M, Sabatini BL, Maylie J, Adelman JP. SK channels and NMDA receptors form a Ca<sup>2+</sup>-mediated feedback loop in dendritic spines. *Nature Neuroscience*. 2005; 8:642–649.
- Nicholson DA, Trana R, Katz Y, Kath WL, Spruston N, Geinisman Y. Distance-dependent differences in synapse number and AMPA receptor expression in hippocampal CA1 pyramidal neurons. *Neuron*. 2006; 50:431–442. [PubMed: 16675397]
- Oren I, Mann EO, Paulsen O, Hajos N. Synaptic currents in anatomically identified CA3 neurons during hippocampal gamma oscillations *in vitro*. *The Journal of Neuroscience*. 2006; 26:9923–9934. [PubMed: 17005856]
- Otmakhova NA, Lisman JE. Contribution of I<sub>h</sub> and GABAB to synaptically induced afterhyperpolarizations in CA1: a brake on the NMDA response. *Journal of Neurophysiology*. 2004; 92:2027–2039. [PubMed: 15163674]
- Otmakhova NA, Otmakhov N, Lisman JE. Pathway-specific properties of AMPA and NMDA-mediated transmission in CA1 hippocampal pyramidal cells. *The Journal of Neuroscience*. 2002; 22:1199–1207. [PubMed: 11850447]
- Perkins KL, Wong RK. Intracellular QX-314 blocks the hyperpolarization-activated inward current I<sub>q</sub> in hippocampal CA1 pyramidal cells. *Journal of Neurophysiology*. 1995; 73:911–915. [PubMed: 7760149]
- Raastad M. Extracellular activation of unitary excitatory synapses between hippocampal CA3 and CA1 pyramidal cells. *The European Journal of Neuroscience*. 1995; 7:1882–1888. [PubMed: 8528462]
- Rall W. Distinguishing theoretical synaptic potentials computed for different soma-dendritic distributions of synaptic input. *Journal of Neurophysiology*. 1967; 30:1138–1168. [PubMed: 6055351]
- Richardson MJE, Silberberg G. Measurement and analysis of postsynaptic potentials using a novel voltage-deconvolution method. *Journal of Neurophysiology*. 2008; 99:1020–1031. [PubMed: 18046003]
- Rolls ET. An attractor network in the hippocampus: theory and neurophysiology. *Learning & Memory*. 2007; 14:714–731. [PubMed: 18007016]
- Smith MA, Ellis-Davies GC, Magee JC. Mechanism of the distance-dependent scaling of Schaffer collateral synapses in rat CA1 pyramidal neurons. *Journal de Physiologie*. 2003; 548:245–258.
- Sokolov MV, Rossokhin AV, MKA, Gasparini S, Berretta N, Cherubini E, et al. Associative mossy fibre LTP induced by pairing presynaptic stimulation with postsynaptic hyperpolarization of CA3 neurons in rat hippocampal slice. *The European Journal of Neuroscience*. 2003; 17:1425–1437. [PubMed: 12713645]
- Spruston N, Jaffe DB, Williams SH, Johnston D. Voltage- and space-clamp errors associated with the measurement of electrotonically remote synaptic events. *Journal of Neurophysiology*. 1993; 70:781–802. [PubMed: 8410172]

- Spruston N, Johnston D. Perforated patch-clamp analysis of the passive membrane properties of three classes of hippocampal neurons. *Journal of Neurophysiology*. 1992; 67:508–529. [PubMed: 1578242]
- Spruston N, Jonas P, Sakmann B. Dendritic glutamate receptor channels in rat hippocampal CA3 and CA1 pyramidal neurons. *Journal de Physiologie*. 1995; 482:325–352.
- Steward O. Topographic organization of the projections from the entorhinal area to the hippocampal formation of the rat. *The Journal of Comparative Neurology*. 1976; 167:285–314. [PubMed: 1270625]
- Stuart G, Sakmann B. Amplification of EPSPs by axosomatic sodium channels in neocortical pyramidal neurons. *Neuron*. 1995; 15:1065–1076. [PubMed: 7576650]
- Talbot MJ, Sayer RJ. Intracellular QX-314 inhibits calcium currents in hippocampal CA1 pyramidal neurons. *Journal of Neurophysiology*. 1996; 76:2120–2124. [PubMed: 8890325]
- Traub RD, Wong RK. Cellular mechanism of neuronal synchronization in epilepsy. *Science*. 1982; 216:745–747. [PubMed: 7079735]
- Urban NN, Barrionuevo G. Active summation of excitatory postsynaptic potentials in hippocampal CA3 pyramidal neurons. *Proceedings of the National Academy of Sciences of the United States of America*. 1998; 95:11450–11455. [PubMed: 9736757]
- Urban NN, Henze DA, Barrionuevo G. Amplification of perforant-path EPSPs in CA3 pyramidal cells by LVA calcium and sodium channels. *Journal of Neurophysiology*. 1998; 80:1558–1561. [PubMed: 9744960]
- Vicini S, Wang JF, Li JH, Zhu WJ, Wang YH, Luo JH, et al. Functional and pharmacological differences between recombinant N-methyl-D-aspartate receptors. *Journal of Neurophysiology*. 1998; 79:555–566. [PubMed: 9463421]
- Weisskopf MG, Nicoll RA. Presynaptic changes during mossy fibre LTP revealed by NMDA receptor-mediated synaptic responses. *Nature*. 1995; 376:256–259. [PubMed: 7617037]
- Williams SH, Johnston D. Kinetic properties of two anatomically distinct excitatory synapses in hippocampal CA3 pyramidal neurons. *Journal of Neurophysiology*. 1991; 66:1010–1020. [PubMed: 1661323]
- Williams SR, Mitchell SJ. Direct measurement of somatic voltage clamp errors in central neurons. *Nature Neuroscience*. 2008; 11:790–798.
- Williams SR, Stuart GJ. Site independence of EPSP time course is mediated by dendritic I(h) in neocortical pyramidal neurons. *Journal of Neurophysiology*. 2000; 83:3177–3182. [PubMed: 10805715]
- Williams SR, Stuart GJ. Role of dendritic synapse location in the control of action potential output. *Trends in Neurosciences*. 2003; 26:147–154. [PubMed: 12591217]
- Witter MP, Amaral DG. Entorhinal cortex of the monkey: V. Projections to the dentate gyrus, hippocampus, and subicular complex. *The Journal of Comparative Neurology*. 1991; 307:437–459. [PubMed: 1713237]
- Wittner L, Miles R. Factors defining a pacemaker region for synchrony in the hippocampus. *Journal de Physiologie*. 2007; 584:867–883.
- Wong RK, Prince DA, Basbaum AI. Intradendritic recordings from hippocampal neurons. *Proceedings of the National Academy of Sciences of the United States of America*. 1979; 76:986–990. [PubMed: 284423]
- Yeckel MF, Berger TW. Feedforward excitation of the hippocampus by afferents from the entorhinal cortex: redefinition of the role of the trisynaptic pathway. *Proceedings of the National Academy of Sciences of the United States of America*. 1990; 87:5832–5836. [PubMed: 2377621]

## Appendix

### Detailed description of sweep categorization

The data sweep parameter extraction method is denoted here in ‘single quotes’, whose values are reported in Table 1. Unless otherwise indicated, times are relative to the stimulus artifact and response values are always treated as positive even for EPSCs. Sweeps showing

a trend slope, either positive or negative, within the ‘pre-stimulation test window’ preceding the stimulus artifact with a magnitude greater than the ‘maximum trend’ were rejected from further processing, as were sweeps showing smoothed values in the ‘pre-stimulation test window’ larger than the ‘minimum peak value’. Sweeps with peak values greater than the “minimum peak” value but estimated latencies lower than the minimum “allowed latency” were similarly rejected from further processing. Single-peak responses were those having a dual-exponential fit with error no greater than the ‘maximum fit error’ and estimated latency, peak time, and HHW within the limits provided by ‘allowed latency’, ‘allowed peak time’, and ‘maximum half-height width’, respectively. Furthermore, single-peak responses should have peak values greater than or equal to the ‘minimum peak value’. Finally, single-peak responses should also have no local peaks larger than the main peak prior to the half-height crossing point, even if the times of such peaks are outside the range of ‘allowed peak time’. Multi-peak sweeps were those not identified as single-peak responses but having peak values in excess of the ‘minimum peak value’ within ‘allowed peak time’ limits and having latencies no greater than the maximum ‘allowed latency’. Sweeps were categorized as failures when the estimated latency was larger than the maximum ‘allowed latency’ and no peaks with values larger than the ‘minimum peak value’ were found prior to the end of the ‘allowed latency’ interval, provided that the minimum-to-maximum range of response values in the time interval from the ‘minimum peak time’ to the maximum ‘allowed latency’ was less than the ‘minimum peak value’. Sweeps not otherwise categorized and meeting the minimum-to-maximum range test for the latency interval were also categorized as failures provided that no peaks were found with values larger than the ‘minimum peak value’. All other cases were categorized as undetermined. See Supplementary Figure 3 for a flowchart of this categorization procedure.

## Mathematical details of fitting procedure

The decay time constant was estimated using a closed-form solution to a method described by Richardson and Silberberg (2008) that minimizes the total variance of a perturbation in an exponentially decaying system. Briefly, the method used here models a decaying response as:

$$\dot{y} = -y/\tau + \varepsilon$$

where  $y$  is the response value (e.g. EPSP) over time,  $\tau$  the decay time constant, and  $\varepsilon$  a random noise source. For values of  $y$  over a given time interval, a value of  $\tau$  is sought that minimizes the total variance of the noise term. The optimal value for  $\tau$  is found as:

$$\tau = \frac{2}{y_0^2 - y_1^2} \int_{t_0}^{t_1} y^2 dt$$

where  $y$  is the EPSP or EPSC value relative to rest,  $t_0$  is the start time of the interval over which the estimate is made,  $t_1$  is the end time,  $y_0$  is the value of  $y$  at  $t_0$ , and  $y_1$  is the value at  $t_1$ .

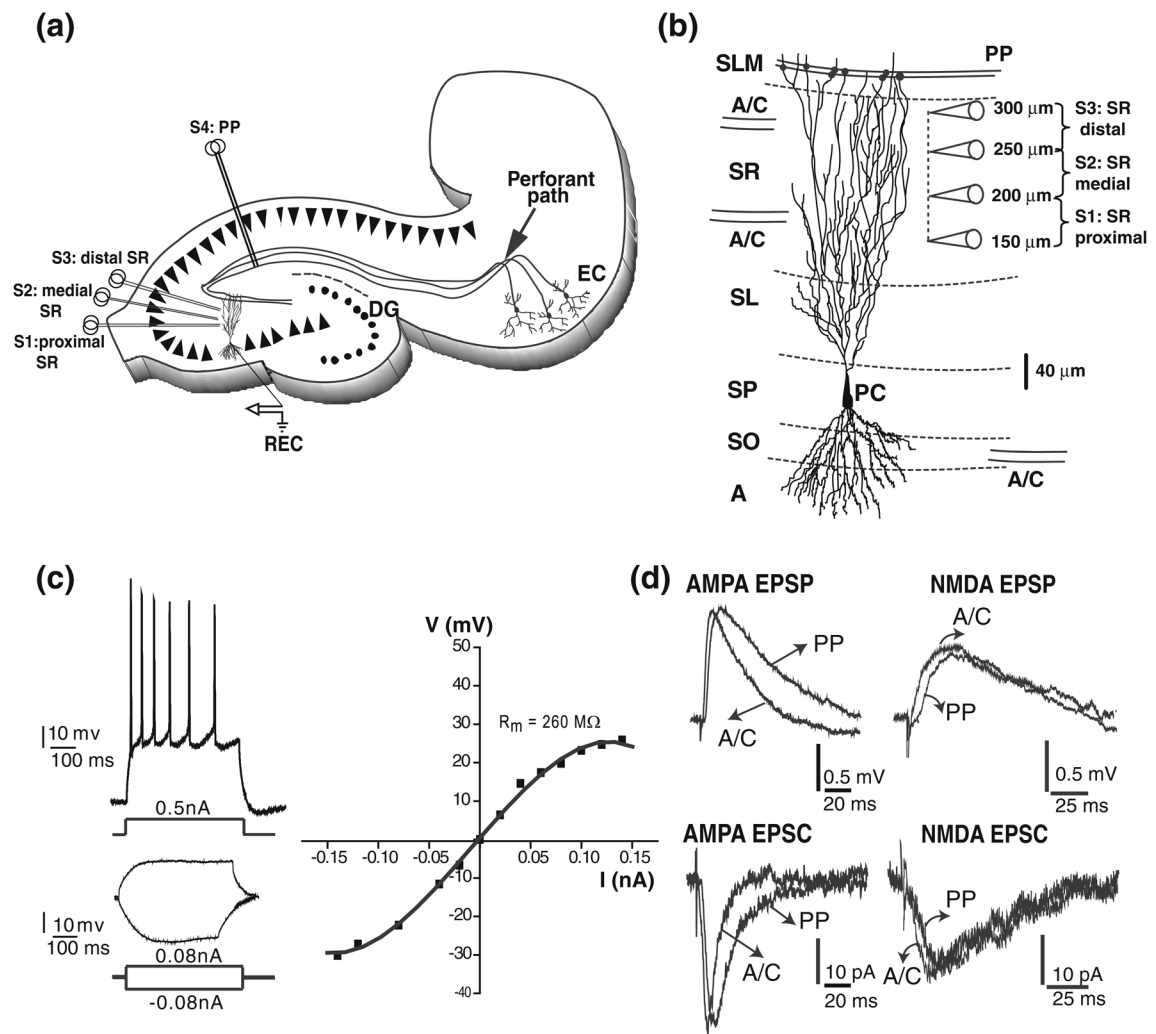
Single-peak responses were identified by fitting the smoothed response to a dual-exponential of the form:

$$y(t) = y_{rest} + a \left[ \exp\left(-\frac{t-b}{\tau_2}\right) - \exp\left(-\frac{t-b}{\tau_1}\right) \right] + \varepsilon_{noise}(t) \text{ if } t > b$$

$$y(t) = y_{rest} + \varepsilon_{noise}(t) \text{ otherwise,}$$

where  $y(t)$  is the response value at a given time,  $y_{rest}$  is the value of the voltage or current at rest,  $t$  is time relative to the stimulus artifact,  $b$  is latency, and  $\tau_1$  and  $\tau_2$  are the rising and falling time constants. The fitting procedure determines values for  $y_{rest}$ ,  $a$ ,  $b$ ,  $\tau_1$  and  $\tau_2$  to minimize the error measure  $\text{var}(e_{noise})/\text{var}(y)$  for  $t$  values over an interval beginning with the pre-stimulation test interval up through a minimum fitting window interval (Table 1) from the peak of the response or up through the trailing half-height crossing, whichever comes last. Fitting was done using the R functions for the Nelder-Mead simplex method except in cases where convergence is not achieved, in which case a quasi-Newton method is also used. To better fit the rising portion of EPSP, an assumed membrane time constant (Table 1) was included in the fitted model in the form of an exponential decay kernel that is convolved with the dual exponential response.

Two latency estimates were derived, one directly from the sweep data and the other from the fitting procedure. For EPSP, the value derived directly from sweep data was more reliable and thus was used in the categorization process, whereas for EPSC, the value derived from the fitting procedure was used. In cases where one of the latency estimates could not be determined, the other was substituted for the purpose of sweep categorizations. Sweeps where no reliable latency estimate was derived were categorized as undetermined.

**Fig 1.**

Firing and subthreshold synaptic responses from CA3 pyramidal cells. **(a)** schematic diagram of hippocampal slice depicting the positions of the concentric bipolar stimulation electrodes (S1–S4). The recording electrode (REC) is in one CA3b pyramidal cell. Associational/commissural fibres (A/C) were activated from the str. radiatum (proximal (S1), medial (S2), distal (S3)). Perforant path fibres (PP) were activated from the str. lacunosum moleculare (S4) in area CA1. **(b)** reconstruction of a CA3 pyramidal neuron showing the typical soma location of CA3pc. CA3 pyramidal cells receive convergent excitatory synaptic inputs from other CA3 pyramidal cells and from the entorhinal cortex, via the A/C and the PP, respectively. The position of the electrodes for proximal, medial, and distal SR stimulations are shown. Abbreviations: A, alveus; SO, str. oriens; SP, str. pyramidale; SL, str. lucidum; SR, str. radiatum; SLM, str. lacunosum-moleculare. **(c)** *Top left:* adapting train of action potentials in response to a high intensity depolarizing current injection in a CA3pc. *Bottom left:* voltage changes in response to low intensity depolarizing and hyperpolarizing current injections in the same CA3pc. *Right:* I–V curve measured from the same CA3pc showing outward and inward rectification. **(d)** Representative AMPA and NMDA subthreshold EPSPs (*top left and right*) and EPSCs (*bottom left and right*) for A/C and PP inputs

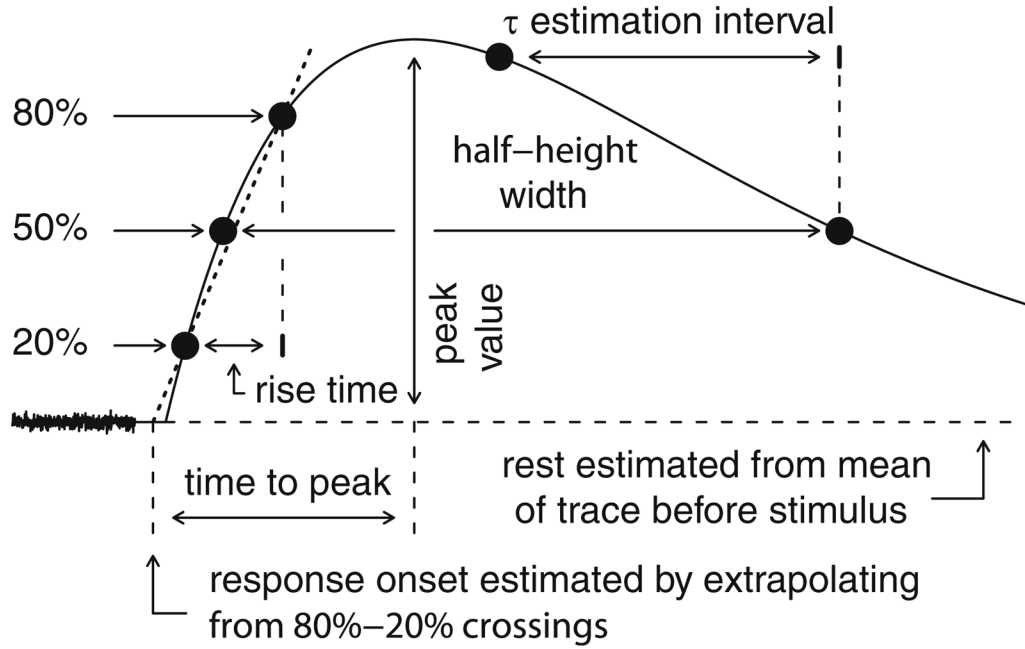


**Fig 2.** Data analysis schematics. Schematic diagram of parameter extraction (see Section 2). Rest is estimated from the mean of un-smoothed data prior to the stimulus artifact. Response onset is estimated from the rising 20% and 80% times and values. Latency is the difference between onset and stimulation times. Peak value is the difference between the actual peak of the smoothed response and rest. Time to peak is the interval between response onset and the peak. Half-height width is the time between the rising and falling 50% times. The decay time constant is estimated over the final 80% of the interval between the peak time and the falling 50% crossing point

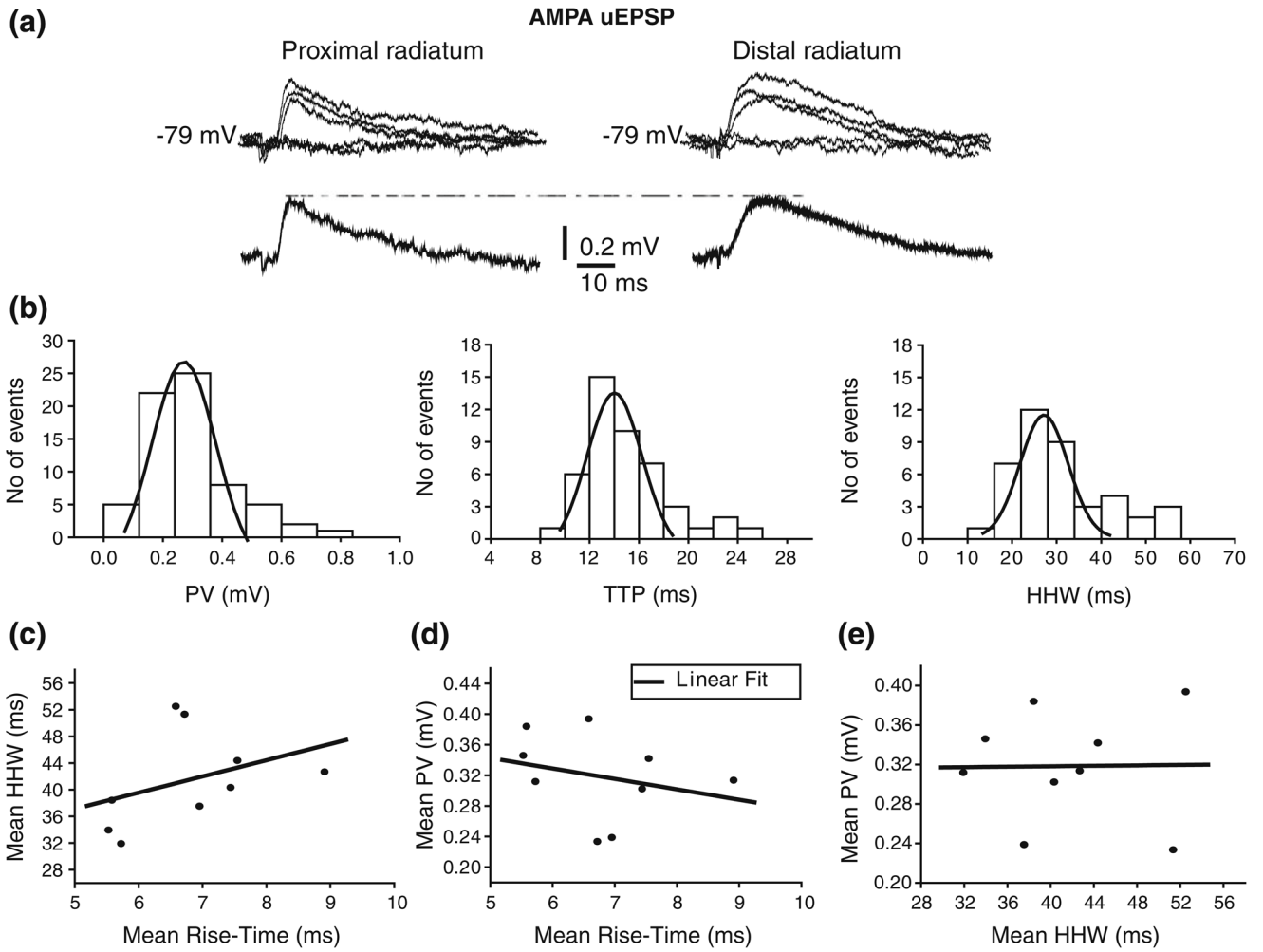


**Fig 3.** Amplitude and kinetic of AMPA uEPSPs evoked from str. radiatum. **(a)** AMPA uEPSPs evoked from proximal (*left traces*) and distal (*right traces*) str. radiatum with corresponding averages underneath. Failures are also depicted but not averaged. **(b)** Intrinsic variability of AMPA uEPSPs evoked from str. radiatum in one cell is shown in histograms for PV (*left*;  $\mu = 0.25 \pm 0.01$  mV), TTP (*center*;  $\mu = 13.8 \pm 0.4$  ms) and HHW (*right*;  $\mu = 26.02 \pm 0.8$  ms). Histograms do not include failures. Low correlation ( $r < 0.4$ ) between mean HHW and rise-time **(c)**, between mean PV and rise-time **(d)**, and between mean PV and HHW **(e)** of AMPA uEPSP evoked from str. radiatum suggest location-independence of amplitudes

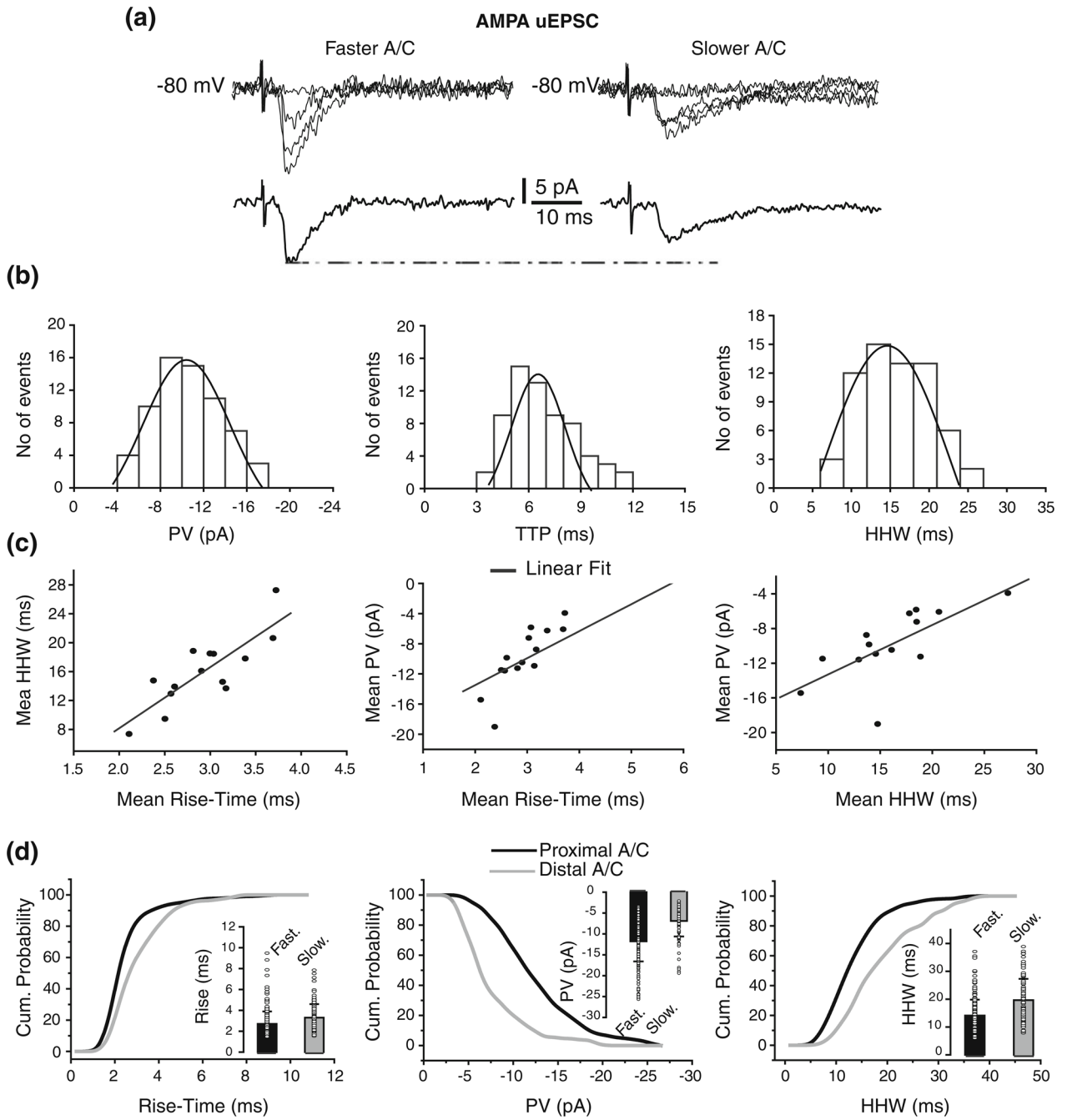


**Fig 4.** Identification of faster and slower A/C uEPSC based on rise-time. **(a)** Fast (*left traces*) and slow (*right traces*) rising AMPA uEPSCs evoked from str. radiatum with corresponding averages underneath. Failures are also depicted but not averaged. **(b)** Peak value (*left*;  $\mu = -10.39 \pm 0.19$  pA), TTP (*center*;  $\mu = 6.2 \pm 0.2$  ms) and HHW (*right*;  $\mu = 15.6 \pm 0.5$  ms) histograms for AMPA uEPSCs evoked from str. radiatum in one cell. Histograms do not include failures. **(c)** High correlations were found between mean HHW and rise-time (*left*), mean PV and rise-time (*center*), and mean PV and HHW (*right*) of AMPA uEPSC evoked from str. radiatum. **(d)** Comparison of cumulative probability distributions for rise-time

(*left*), PV (*center*), and HHW (*right*) of fast and slow rising AMPA uEPSC evoked from str. radiatum reveals putative proximal and distal A/C synapses. Significant differences were found in rise-time ( $p < 0.02$ ), PV ( $p < 0.02$ ), and HHW ( $p < 0.05$ ) between AMPA uEPSC from proximal vs. distal A/C. Insets: Mean and s.d. of the unitary values (*circle*) for rise-time (*left*), PV (*center*), and HHW (*right*)

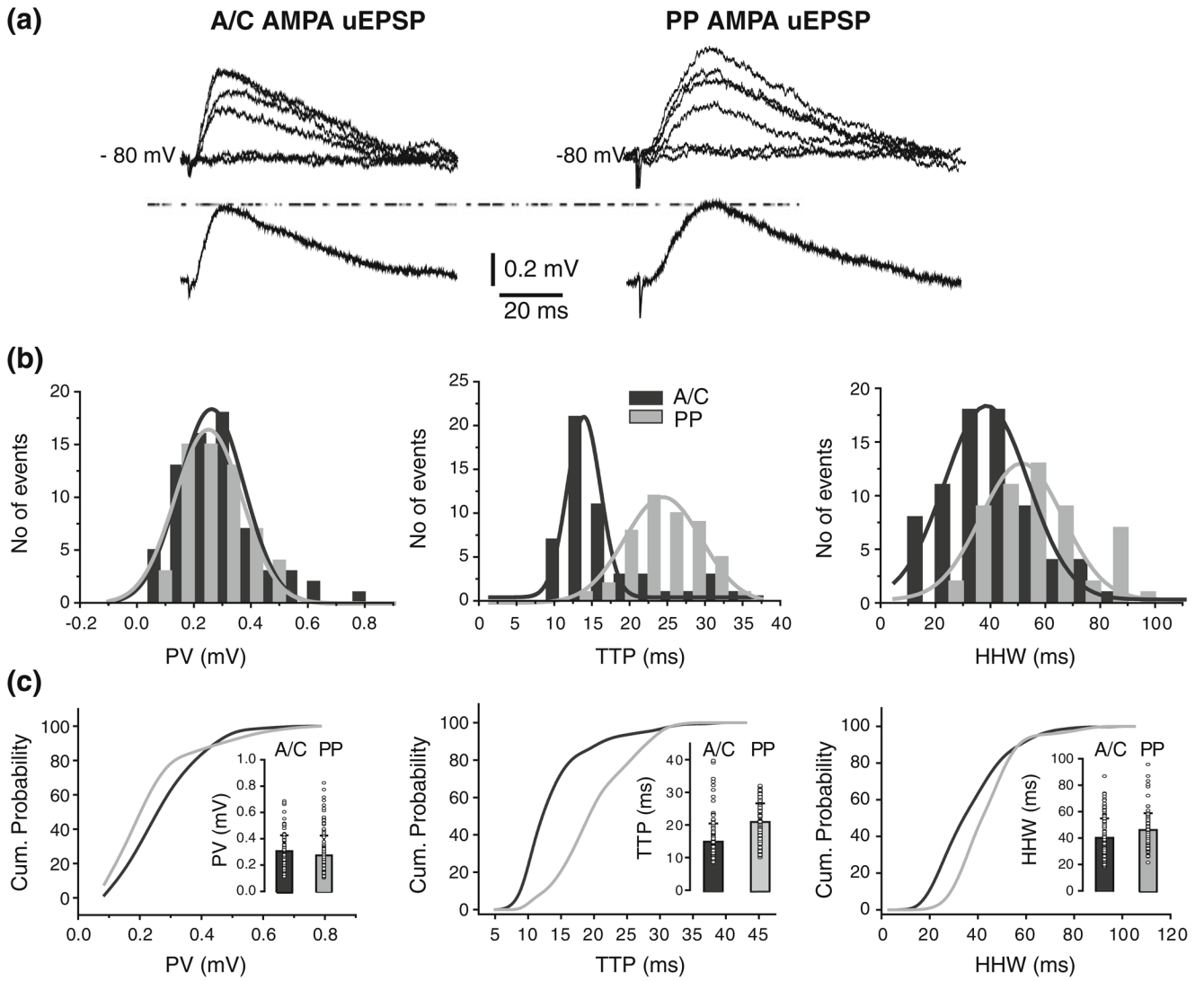


**Fig 5.** Location-independence of somatic A/C and PP AMPA uEPSP amplitudes. **(a)** AMPA uEPSP from A/C (*left*) and PP (*right*), with corresponding averages underneath. Failures are also depicted but not averaged. **(b)** Peak amplitude (*left*), TTP (*center*) and HHW (*right*) histograms for A/C AMPA uEPSPs (*black*), and for PP AMPA uEPSPs (*gray*) in one cell. Histograms do not include failures. **(c)** Comparison of cumulative probability distributions for PV (*left*), TTP (*center*), and HHW (*right*) from A/C (*black*) and PP (*gray*) AMPA uEPSPs. Insets: Mean and s.d. of the unitary values (*circle*) for PV (*left*), TTP (*center*), and HHW (*right*). A significant difference was found in TTP ( $p < 0.001$ ), but not in PV or HHW, between AMPA uEPSC from A/C vs. PP

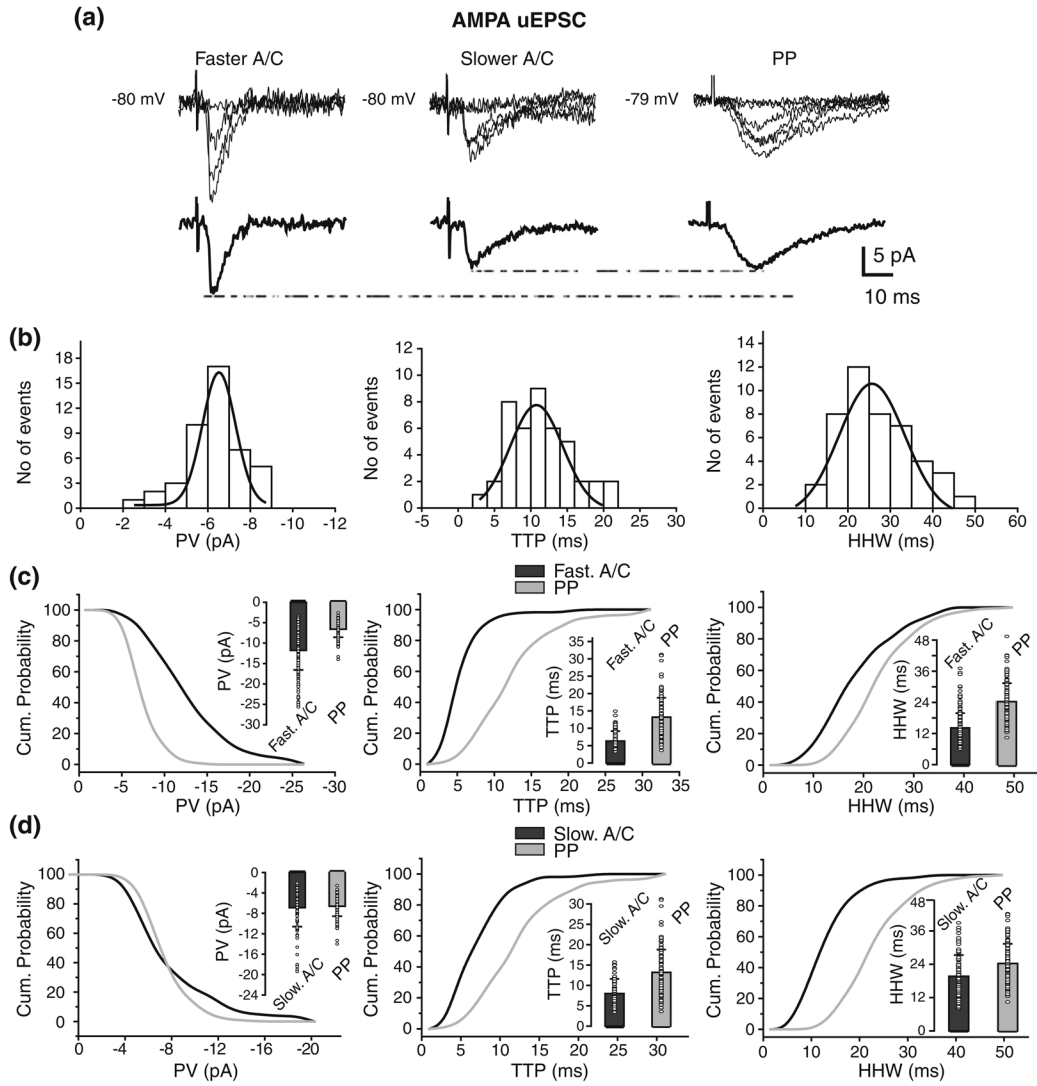


**Fig 6.** Voltage clamp reduces the location-independence of A/C and PP uEPSP amplitudes. **(a)** AMPA uEPSCs generated from faster A/C (*left*), slower A/C (*center*), and PP (*right*) synapses with corresponding averages underneath. **(b)** Variability of PP AMPA uEPSC is shown in histograms for PV (*left*;  $\mu = -6.4 \pm 0.1$  pA), TTP (*center*;  $\mu = 10.5 \pm 0.6$  ms) and HHW (*right*;  $\mu = 24.7 \pm 1.2$  ms) from one cell. Comparison of the cumulative probability distributions for PV (*left*), TTP (*center*), and HHW (*right*) of AMPA uEPSCs from PP and faster **(c)** or slower **(d)** A/C synapses. Amplitude distribution for faster A/C uEPSC is shifted to the right whereas slower is not when compared to PP. Significant differences were found in PV ( $p < 0.02$ ), TTP ( $p < 0.001$ ), and HHW ( $p < 0.001$ ) between AMPA uEPSC from faster A/C vs. PP. However, no significant difference was found in PV between AMPA uEPSC from slower A/C vs. PP. Insets: mean and s.d. of the unitary values (*circle*) for PV (*left*), TTP (*center*), and HHW (*right*) of PP AMPA uEPSCs and those from faster (putative proximal; **(c)**) or slower (putative distal, **(d)**) A/C

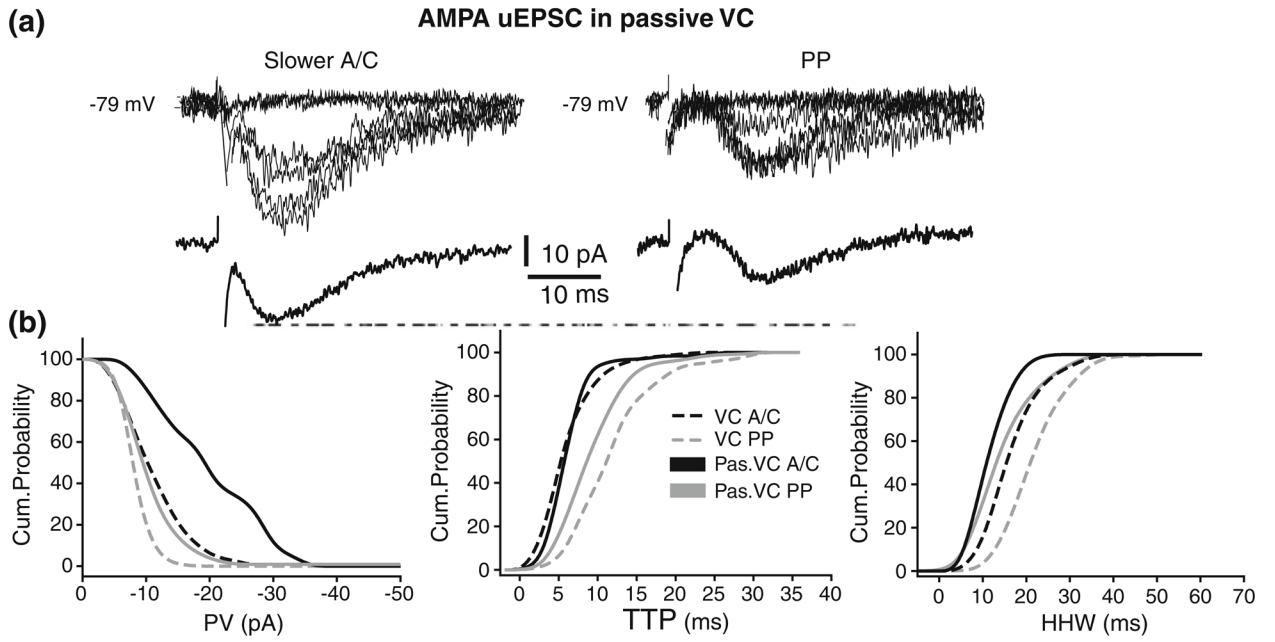


**Fig 7.** Blockade of voltage-dependent conductances reveals dampening of distal A/C EPSCs. AMPA uEPSC from slower (putative distal) A/C (*left*) and PP (*right*) in passive VC conditions (**a**). (**b**) Comparison of cumulative probability distributions for PV (*left*), TTP (*center*), and HHW (*right*) from A/C and PP in VC (A/C, black dashed line; PP, gray dashed line) and passive VC (A/C, black; PP, gray) conditions. Shift to the right in the PV distribution of distal A/C vs. PP uEPSC in passive VC (*black vs. gray*;  $p < 0.05$ ) and of distal A/C uEPSC in passive VC vs. VC (*black vs. black dashed line*;  $p < 0.02$ ) suggest dampening of slower A/C uEPSC in VC

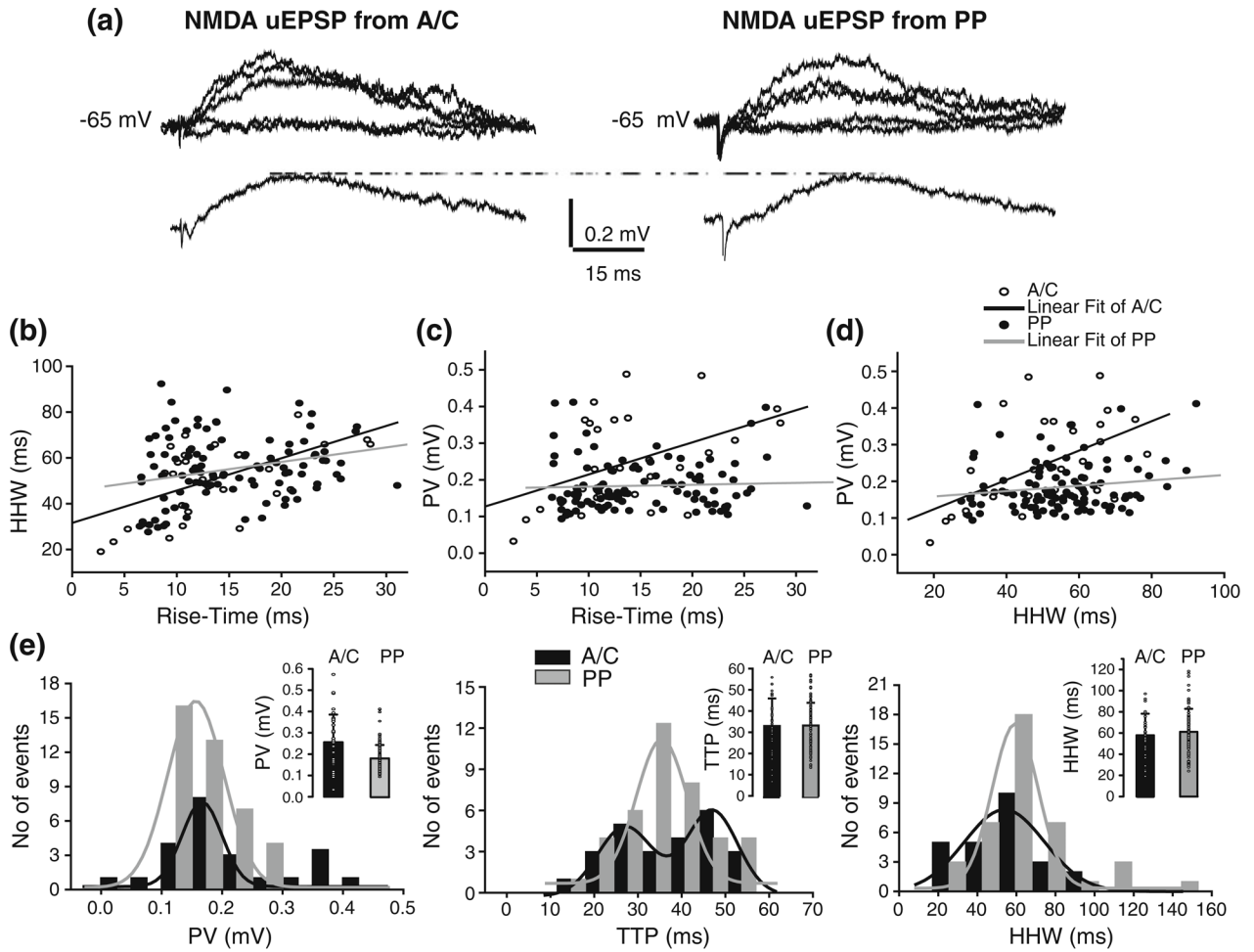


**Fig 8.** Location-independence of somatic A/C and PP NMDA uEPSP. **(a)** NMDA uEPSPs from str. radiatum A/C (*left traces*) and PP (*right traces*) with corresponding averages at the bottom. Failures are also depicted but not averaged. **(b)** Filtering of NMDA uEPSP from str. radiatum A/C (*open circle*) or from PP (*closed circle*) as indicated by the correlation between mean HHW and rise-time. Both mean PV vs. rise-time **(c)** and mean PV vs. HHW **(d)** show strong correlation for A/C but not for PP NMDA uEPSP. **(e)** Peak value (*left*), TTP (*center*) and HHW (*right*) histograms for NMDA uEPSPs evoked from A/C (*black*) and PP (*gray*). No significant differences were found in PV, TTP, and HHW between NMDA uEPSP from A/C vs. PP. Histograms do not include failures. Insets: Mean and s.d. of the unitary values (*circle*) for PV (*left*), TTP (*center*), and HHW (*right*) of A/C (*black*) and PP (*gray*) AMPA uEPSCs

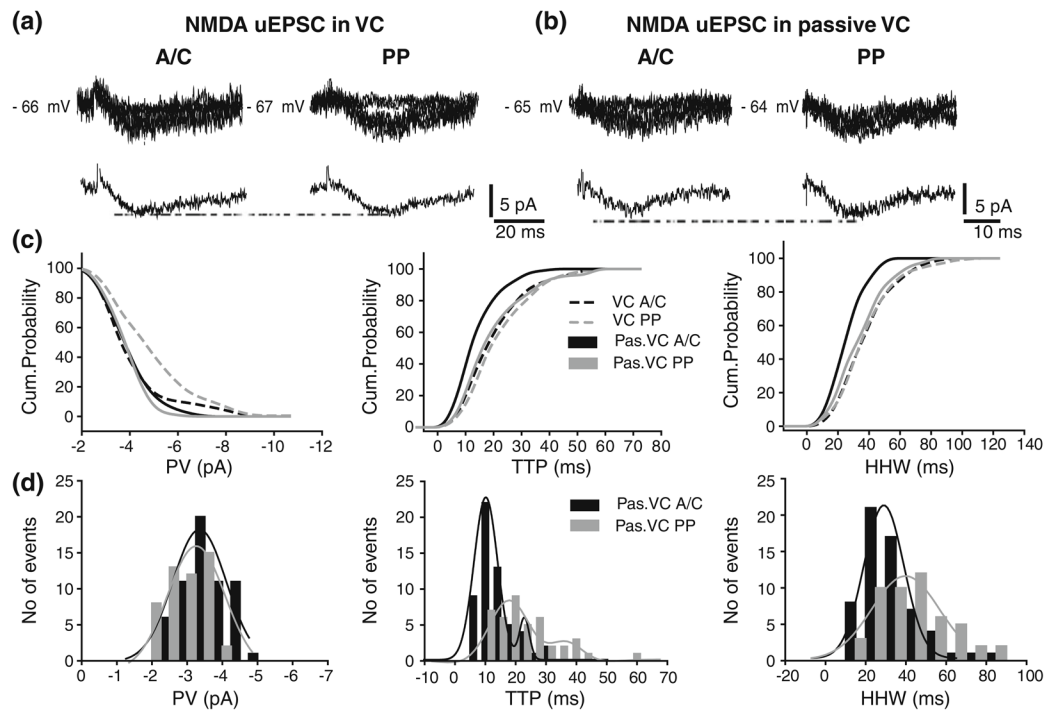


**Fig 9.** Location-independence of somatic A/C and PP NMDA uEPSC. AMPA uEPSC from A/C (*left*) and PP (*right*) in VC (**a**) and passive VC conditions (**b**) with corresponding average traces underneath. Failures are also depicted but not averaged. (**c**) Comparison of cumulative probability distributions for PV (*left*), TTP (*center*), and HHW (*right*) from A/C and PP NMDA uEPSP in VC and in passive VC conditions. No significant differences were found in amplitude and kinetic parameters. (**d**) Peak value (*left*), TTP (*center*) and HHW (*right*) histograms for A/C and PP AMPA uEPSPs recorded from one cell in passive VC condition. Histograms do not include failures

**Table 1**

Data analysis parameters and thresholds

Parameter or threshold	CC		VC	
	AMPA	NMDA	AMPA	NMDA
Pre-stimulation test window (ms)	15	15	10	10
Maximum trend (mV ms <sup>-1</sup> or pA ms <sup>-1</sup> )	0.01	0.01	0.5	0.5
Minimum peak value (mV or negative pA)	0.10	0.10	2.0	2.0
Allowed latency (ms)	-5-15	-5-15	-5-10	-5-10
Allowed peak time (ms)	5-40	5-60	5-40	5-60
Minimum fitting window (ms)	40	40	30	30
Maximum fit error (non-dimensional)	0.10	0.10	0.10	0.15
Smoothing cutoff frequency (Hz)	60	60	180	100
Maximum half-height width (ms)	100	200	50	150
$\tau_m$ assumed for fitting (ms)	20	20	0	0

**Table 2**

Somatic amplitude and kinetic parameters from A/C and PP AMPA uEPSP

	A/C str. radiatum	A/C str. oriens	PP
PV (mV)	0.3±0.1	0.3±0.1	0.3±0.1
Range	0.1–0.7	0.1–0.7	0.1–0.8
TTP (ms)	15.8±5.7	13.7±5.3	20.9±5.7
Range	9.0–39.1	7.7–39.7	10.1–35.7
Rise-time (ms)	7.1±3.2	6.5±2.7	9.1±3.0
Range	4.2–24.0	4.1–24.2	4.5–24.0
HHW (ms)	40.9±15.3	38.0±13.6	46.1±12.7
Range	14.0–87	15.8–98.4	21.4–96.0
Decay-time (ms)	43.0±19.3	41.7±19.0	45.2±16.3
Range	11.1–98.0	12.6–94.0	15.6–104.0

**Table 3**  
Somatic amplitude and kinetic parameters from A/C and PP AMPA uEPSCs in VC and passive

Parameter	VC			Passive VC		
	Faster A/C	Slower A/C	A/C str. oriens	PP	Slower A/C	PP
PV (pA)	-11.8±4.8	-6.9±3.7	-8.1±3.4	-6.6±2.0	-18±8.1	-9.0±5.6
Range	3.5 to -25.6	-2.1 to -19.4	-2.2 to -19.4	-2.6 to -14	-5.1 to -33.3	-2.8 to -50.7
TTP (ms)	6.1±2.1	7.7±3.0	6.7±2.8	13.2±5.6	7.5±3.2	10.5±4.5
Range	3.2-14.9	3.4-15.8	3.1-18.4	4.0-31.2	3.2-25.7	3.8-29.6
Rise-time (ms)	2.7±1.2	3.3±1.3	3.1±1.6	6.6±4.0	4.8±3.0	5.1±3.0
Range	1.5-9.5	1.5-8.0	1.4-11.2	1.5-23.0	1.4-20.3	1.7-19.1
HHW (ms)	14.1±5.7	19.7±7.6	15.7±6.2	24.3±7.1	13.6±4.1	19.1±6.4
Range	5.9-37.0	7.9-38.9	4.5-37.0	10.4-49.4	7.9-24.8	8.6-39.5
Decay-time (ms)	13.7±6.4	21.9±11.5	17.0±10.2	25.0±11.4	12.5±5.7	18.9±9.8
Range	4.3-45.8	5.8-56.3	3.3-59.0	9.6-71.7	4.9-40.8	4.5-55.0

**Table 4**  
Somatic amplitude and kinetic parameters from A/C and PP NMDA uEPSP/uEPSC

Parameter	CC		VC		Passive VC	
	A/C str. radiatum	PP	A/C str. radiatum	PP	A/C str. radiatum	PP
PV (mV or pA)	0.3±0.1	0.2±0.1	-3.8±1.7	4.5±1.7	-3.5±1.0	-3.5±0.8
Range	0.1-0.6	0.1-0.4	-1.8 to -9.2	-2.1 to -10.5	-1.9 to -6.4	-2.1 to -5.5
TTP (ms)	32.9±13.0	33.2±10.7	22.0±11.1	23.8±11.2	16.0±7.7	21.8±12.1
Range	6.7-55.8	13.2-57.0	5.2-57.7	6.1-57.7	6.0-40.2	6.3-57.3
Rise-time (ms)	15.8±7.7	16.1±7.3	11.1±6.9	12.4±7.0	9.2±6.1	12.3±9.6
Range	2.7-32.6	6.4-39.2	2.1-39.9	2.4-40.5	2.6-27.8	2.8-45.8
HHW (ms)	57.9±20.3	61.1±21.7	41.3±17.5	41.4±19.0	28.6±10.8	37.7±17.0
Range	19.2-97.0	24.0-152.0	10.4-98.0	9.0-108.0	11.4-55.2	9.2-81.6
Decay-time (ms)	52.9±30.3	63.7±34.7	46.2±27.3	46.3±29.9	30.3±19.1	42.6±30.5
Range	16.3-136.0	12.4-165.0	5.7-113.0	6.0-137.0	6.0-96.9	6.4-124.0